



# SAPHYRE

## Contract No. FP7-ICT-248001

## System Level Performance Evaluation
## D4.4

| | |
|---|---|
| Contractual date: | M36 |
| Actual date: | M36 |
| Authors: | Leonardo Badia, Francesco Guidolin, Martin Schubert, Osman Aydin, Stefan Valentin, Torsten Fahldieck, Eleftherios Karipidis, Michał Szydełko, Jarosław Byrka, Jakub Oszmiański, Jianshu Zhang, Haibin Zhang, Remco Litjens |
| Participants: | ALUD, CFR, FhG, LiU, TNO, TUIL, WRC |
| Work package: | WP4 |
| Security: | Public |
| Nature: | Report |
| Version: | 1.3 |
| Number of pages: | 63 |

**Abstract**

This deliverable reports on the system level evaluations performed by the SAPHYRE project to quantify the performance gain of spectrum and infrastructure sharing (also dubbed "SAPHYRE gain") from a system level perspective. The analysis includes both advanced physical layer enablers of the sharing paradigm and network evaluation of the upper layers in realistic scenarios. The deliverable details several aspects of the sharing concept, including resource allocation in multi-user multi-operator network scheduling, relaying, and full sharing. The main result of our evaluations is a general benefit of sharing resources which, in realistic scenarios appears to be higher than 15% and can become significantly higher if proper conditions are met.

**Keywords**

Full sharing, infrastructure sharing, spectrum sharing, LTE HSPA, system level evaluation.

# Contents

# Abbreviations

| | |
|---|---|
| 3G-LTE | 3GPP Long Term Evolution |
| 3GPP | Third Generation Partnership Project |
| AP | Auctioning Process |
| AU | Auctioning Unit |
| AUC | AU Carriers |
| AWGN | Additive White Gaussian Noise |
| BC | Broadcast Channel |
| BS | Base Station |
| CDF | Cumulative Distribution Function |
| CDMA | code-Division Multiple Access |
| CS/CB | Coordinated Scheduling/Beamforming |
| CSI | Channel State Information |
| CU | Central Unit |
| CoMP | Coordinated Multi-Point |
| DL | Downlink |
| E-UTRAN | Enhanced UMTS Terrestrial Radio Access Network |
| eNB | Evolved Node B |
| FDMA | Frequency Division Multiple Access |
| FSA | Fixed Spectrum Alignment |
| GSM | GLOBAL SYSTEM for Mobile Communications |
| HSOPA | High Speed OFDM Packet Access |
| HSPA | High Speed Packet Access |
| ISI | Inter-Symbol interference |
| ITU | International Telecommunications Union |
| LTE | Long Term Evolution |
| LTE-A | Long Term Evolution - Advanced |
| MAC | Medium Access Control |
| maxSINR | Maximum SINR |
| MIMO | Multiple-Input Multiple-Output |
| MISO | Multiple-Input single-Output |
| ML | Maximum Likelihood |
| MMSE | Minimum Mean Square Error |
| MNO | Mobile Network Operator |
| MRC | Maximum Ratio Combining |
| MRT | Maximum Ratio Transmission |
| MSE | Mean Square Error |
| MU | Multi-User |
| MU-CDSA | Multi-User Channel-Dependent Scheduling Algorithm |
| MU-MIMO | Multi-User MIMO |
| MU-MUX | Multi-User Spatial Multiplexing |

| | |
|---|---|
| MU-SDMA | Multi-User Space-Division Multiple Access |
| NS3 | Network Simulator 3 |
| OFDM | Orthogonal Frequency Division Multiplex |
| OFDMA | Orthogonal Frequency Division Multiple Access |
| OPEX | OPerating Expenditures |
| PF | Proportional Fair |
| PHY | Physical Layer |
| PRB | Physical Resource Block |
| QoS | Quality of Service |
| RAT | Radio Access Technology |
| RB | Resource Block |
| RS | Relay Station |
| SCME | Spatial Channel Model Extended |
| SDMA | Spatial Division Multiple Access |
| SIMO | Single-Input Multiple-Output |
| SINR | Signal-to-Interference-and-Noise Ratio |
| SISO | Single-Input Single-Output |
| SNR | Signal-to-Noise Ratio |
| SU | Single-User |
| SU-MIMO | Single-User MIMO |
| TDMA | Time Division Multiple Access |
| TLS | Two Layered Scheduler |
| TTI | Transmission Time Interval |
| UE | User Equipment |
| UL | Uplink |
| UMTS | Universal Mobile Telecommunications System |
| VCG | Vikrey, Clarke and Groves |
| ZF | Zero-Forcing |

# 1 Executive Summary

With the rapid growth of the number of mobile terminals, and the constantly increasing demand for the mobile services at high data rates, the limitation of spectrum allocation is becoming the bottleneck for many cellular network operators. Therefore, physical radio resources sharing, as well as infrastructure sharing, has been widely considered for the future of wireless communications, both to overcome the scarcity of spectrum, and to decrease Operational Expenses (OPEX) of cellular networks [1, 2].

Spectrum might be shared by users of multiple operators either orthogonally [3, 4] or non-orthogonally [5] in a coordinated manner. By orthogonal spectrum sharing, user terminals (UEs) of different operators are scheduled to avoid simultaneous use of the same frequency at small timescale (e.g. milliseconds to minutes). In this case spectrum is still shared among operators at relatively large timescales (e.g. hours, days). This differs from fixed spectrum assignment (FSA), where a certain frequency is only accessible by users of one single operator. By non-orthogonal spectrum sharing, UEs of multiple operators are allowed to use the same frequency simultaneously and thus potentially interfere with each other.

It is the purpose of this study to quantitatively evaluate the performance of resource allocation strategies and techniques considered in full sharing scenarios. The important challenge of our studies is to derive *system level* evaluations, i.e. comprehensive of all the layers of the protocol stack and depicting realistic scenarios with multiple terminals and operators, if applicable.

We propose numerical assessments, where we report in extensive detail the evaluation instruments, i.e. system simulators described, whenever possible, openly and comprehensively and available for reproducibility and scientific validity of the results. Moreover, we aim at deriving numerically consistent quantifications of the so-called "SAPHYRE" gain, i.e. an evaluation of the benefit of exploiting infrastructure and spectrum sharing techniques with respect to traditional allocation without any sharing.

The following chapters present separate contributions which have been arranged in an organic fashion to cover all the system level evaluation aspects of the SAPHYRE project. In more detail, in Chapter 2 we focus on the system level analysis of a Two Layered Scheduler that efficiently schedules data for multiple operators sharing time slots, and allowing for dynamic scheduling policies. This is the enabler of further system level resource sharing paradigms, such as the analysis of a broker-based spectrum sharing presented in Chapter 3. A detailed characterization of lower layers together with transport optimization is introduced in the following chapters, so that Chapter 4 elaborates the evaluation of transmit beamforming on spectrum allocation with shared resources. Chapter 5 extends this concept further to the so-called *full sharing*, i.e. by combining spectrum and infrastructure resource sharing, i.e. by generating a whole distributed MIMO system where the base stations belonging

to different operators cooperate as well. Then, Chapter 6 presents a detailed and thoroughly evaluation campaign of all the tested scenarios in an open source system level evaluator, a customized version of the well-known ns-3 simulator, which has been described in the previous deliverables. Finally, Chapter 7 also covers another aspect of infrastructure sharing, i.e. the introduction of shared relays to increase transmission efficiency.

# 2 Two Layered Scheduler for Full Sharing Scenario

It becomes key for the network operators to pursue an efficient exploitation of the wireless medium, both in the sense of using advanced physical layer techniques, and also to seek coordination among each operator. To do so, operators and infrastructure providers agree on a fixed sharing ratio that has to be guaranteed during operation. In traditional approaches, each operator receives a fraction of the overall bandwidth that is proportional to the sharing ratio. At a first glance, such bandwidth splitting is appealing. It is simple and the allocated resource fraction is guaranteed. However, allocating fixed sub-bands leads to a mismatch between sharing ratio and operator cell capacity in frequency-selective propagation scenarios. Moreover, due to the fixed bandwidth limit, the cell capacity of one operator may be too low to support the current traffic while sufficient bandwidth is available in the sub-band of another operator. This artificially created bottleneck wastes resources and reduces service quality in bursty traffic scenarios. To avoid such shortcomings, the whole bandwidth is cyclically allocated among the operators. Sharing time slots instead of spectrum allows the currently scheduled operator to cope with bursty traffic. Following a simple Round Robin (RR) policy holds the agreed sharing rates by adjusting the duration of time slots. While RR is performed in the first step, each operator can execute its own scheduling policy in step 2. This flexibility is a significant benefit of this Two-Layered Scheduler (TLS) design.

## 2.1 System Model Scenario

We study the downlink of a single cell covered by one Base Station (BS). We denote the set of operators by $\mathcal{J}$ and the set of active users in the cell as $\mathcal{K}$. The BS is shared among $\mathrm{J} = |\mathcal{J}|$ network operators and the number of active users is $\mathrm{K} = |\mathcal{K}|$. The system bandwidth is denoted as B and shared among the users of a single operator.

## 2.2 Channel and Traffic Assumptions

To obtain tractable results, we assume a simple fading model where the channel coefficient $h_k[n]$ of an arbitrary $k$th user and $n$th time slot is a circularly symmetric complex Gaussian random variable. This random variable is independent and identically distributed (i.i.d.) among time slots and users.

This classic Rayleigh fading model ([6], Sec. 2.4.2) leads to the i.i.d. exponentially distributed instantaneous Signal-to-Noise Ratio (SNR)

$$\gamma_k[n] = |h_k[n]|^2 \, \mathrm{SNR}_k \tag{2.1}$$

where $\mathrm{SNR}_k$ is the average SNR given by the $k$th user path loss and shadowing. We calculate the Physical layer (PHY) rate an arbitrary user $k$ achieves per time

slot using Shannon's equation as $r_k = \log_2(1 + \gamma_k)$.

To focus on scheduler operation, we exclude further dynamics from our study. To this end, we assume the full buffer traffic model. Here, the downlink transmission at the BS is filled during the complete simulation time for each user in $\mathcal{K}$. This simple traffic model corresponds to the download of a large file and creates a constant load. We vary K to study our system for different loads.

## 2.3 Scheduling Assumptions

From the set of active users the user set $\mathcal{K}^* \subseteq \mathcal{K}$ is scheduled. We denote the number of scheduled users as $k_{max} = |\mathcal{K}^*|$ and assume that each scheduled user receives the fraction $B/k_{max}$ of bandwidth B. The duration of a scheduling period, within which the users of all J operators are scheduled is given by $T$.

An important building block for our inter-operator scheduler is the Round Robin (RR) policy, where the resource allocation is exclusive and alternates among the requesting entities. We employ this simple strategy for inter-operator scheduling in the first stage of our algorithm and study it as one possible option for inter-user scheduling. Here, several scheduling policies are possible. In this paper, we focus on the widely-used class of Proportional Fair (PF) schedulers, which assigns resources to those users $k_{max}$ with the highest weight

$$\lambda_k(n) = \frac{[r_k(n)]^\alpha}{[R_k(n)]^\beta} \tag{2.2}$$

in the current time slot. In 2.2, $\alpha \in [0, \infty[$ and $\beta \in [0, \infty[$ are constant parameters to adjust the effect of the corresponding terms. The quantity $R_k(n)$ is the moving average over time, which is calculated as

$$R_k(n) = \begin{cases} (1-\theta)R_k(n-1) + \theta r_k & k \in \mathcal{K}^* \\ (1-\theta)R_k(n-1) & k \notin \mathcal{K}^* \end{cases} \tag{2.3}$$

where the constant forgetting factor $\theta$ allows to trade off average and update.

In addition to PF scheduling, we compare our TLS multi-operator scheduler to Maximum Rate (MAX) scheduling for users of a single operator. With this scheduling policy, weight 2.2 reduces to $\alpha_k(n) = r_k(n)$, i.e. the first $k_{max}$ users with the highest instantaneous PHY rate are scheduled.

## 2.4 Two Layered scheduler Architecture

As illustrated in Fig. 3.1, our Two-Layered Scheduler (TLS) consists of two phases. In the first phase, radio resources are assigned among operators following the RR strategy. Thus, one after the other, each operator gets exclusive access to the channel once per scheduling period. The number of allocated time slots $\Delta n_j$ depends on the sharing rate of operator $j$. Details on this first phase will be provided below.

In phase 2, the scheduled operator allocates the channel resources among its users. Here, each operators can implement an individual scheduling policy, without affecting the inter-user scheduling of other operators.

This scheduling architecture can be facilitated by providing an Application Programming Interface (API) for the inter-user schedulers to the operators. Moreover, it can be used in other hierarchical scenarios such as heterogeneous networks, where each cell size would be reflected by one stage.

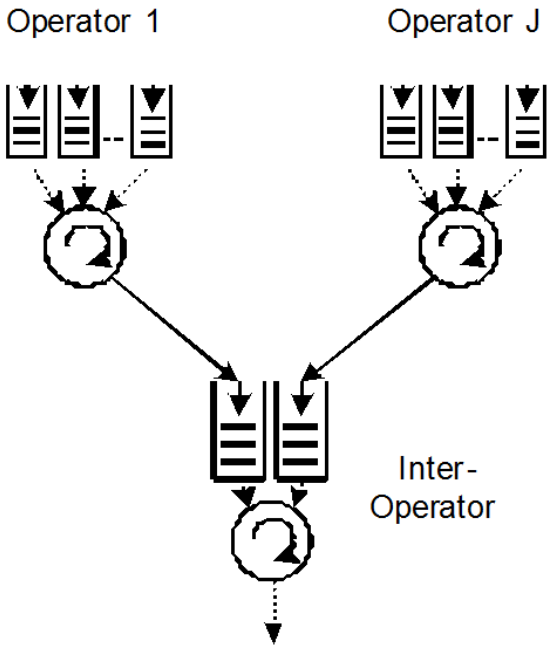


Figure 2.1: Two-Layerd Scheduler (TLS) architecture for J operators

## 2.5 Scheduling Algorithm

The procedure of the scheduling algorithm follows the two phases discussed above but can be implemented as nested loops.

| | |
|---|---|
| Set of sharing operators | $\mathcal{J}$ |
| Set of active users | $\mathcal{K}$ |
| Operator's sharing ratio | $\mathbf{g} := (g_1, \ldots, g_J)$ |
| Duration of scheduling period | T |
| Users' instantaneous SNR | $\gamma := (\gamma_1, \ldots, \gamma_K)$ |
| Proportional Fairness parameters | $\alpha, \beta$ |
| Number of scheduled users per time frame | $k_{max}$ |
| Bandwidth | B |
| Allocated rate matrix | $\mathbf{S} \in \mathrm{Re}^{J \times K}$ |

In the first scheduling phase, we grant each operator a fraction $g_j$ of the scheduling period duration T. Applying a floor function provides the number of time slots $\Delta n_j$ for an arbitrary operator $j$. In the second phase, this number of slots is allocated

to each operator following the Round Robin principle. Within each time slot, an operator performs its own policy to schedule its users. We choose the Proportional Fair policy as a widely-used example. The algorithm returns the matrix $\mathbf{S}$, which includes non-zero rates for the scheduled users of all operators. The algorithm operation is illustrated in Fig. 3.2 [7]. Per scheduling period, each operator $j \in \mathcal{J}$ receives $\Delta n_j$ time slots. After J of such allocations, a new scheduling period starts. Two of such periods are illustrated in Fig. 3.2. Note that sequentially scheduling operators, adds communication delay. This delay can be statistically equal distributed among the operators by randomly reordering the elements in the operator set $\mathcal{J}$ between two scheduling periods. The complexity of the algorithm is dominated by a sort function. Thus, its complexity is $\mathcal{O}(\mathrm{K} \log \mathrm{K})$ in most cases. This is equal to PF and MAX scheduling and practical for a typical number of users.

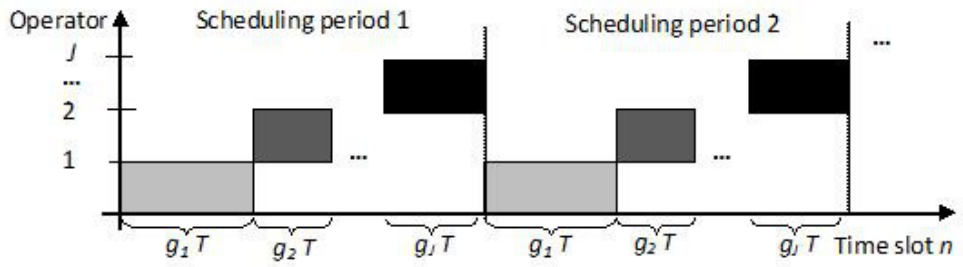


Figure 2.2: Example operation of TLS: Round Robin scheduling of J operators

## 2.6 Simulation Results

We now study how multi-operator TLS performs compared to common single-operator schedulers such as PF, MAX, and RR. After comparing data rate and fairness, we focus on the specifics of multi-operator scheduling. In particular, we study if TLS keeps the agreed sharing ratios and by how much multi-operator scheduling in time increases the delay.

### 2.6.1 Simulation Parameters

We study data rate, sharing ratio and delay for several values of SNR. At each simulation drop of $1s$, the SNR is randomly generated within a practical interval (cp. Table 2.1). Fig. 3.3 shows the resulting Cumulative Distribution Function (CDF), also known as Geometry.

To account for different traffic loads, we study two numbers of active users. While 30 users correspond to a typical load, 100 users refer to a highly loaded cell. As we study $\mathrm{J} = 2$ operators for TLS, each operator receives 15 or 50 users, respectively. Further parameter values are summarized in Table 2.1. All schedulers are studied under equal assumptions.

Table 2.1: Simulation Parameters.

| Parameter | Value | |
|---|---|---|
| **Simulated time** | Simulated time: | $200s$ |
| **Network Parameters** | Number of users: | $30, 100$ |
| | Number of operators: | $1, 2$ |
| | Number of cells: | $1$ |
| | Operator ratios: | $0.5, 0.75, 0.9$ |
| | Nr. of scheduled users: | $6$ |
| **Scheduler** | PF and TSS: | $\alpha = 1$ |
| | | $\beta = 0.5$ |
| | | $* = 0.5$ |
| **Channel Model** | SNR range: | $[-5dB, +20dB]$ |
| **Statistical evaluation** | Evaluation period: | $1s$ |

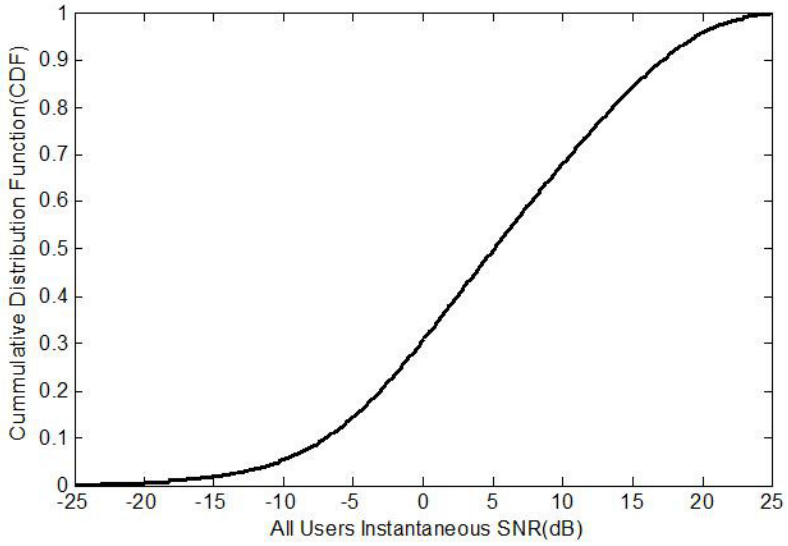


Figure 2.3: Cumulative Distribution Function of the variable SNR.

### 2.6.2 Data Rate

The scatter plot in Fig. 2.4 provides a first impression on the fairness and average sum rate. The latter metric is the time-average of the aggregated downlink rates over all users in the system and points to the average throughput of the system. Fairness is measured as the 5% Quantile of the data rates, which expresses the throughput of users at the cell edge. As shown, the performance of TLS is similar to applying the PF policy to users of a single operator. Constant performance values are achieved also with hanging network conditions. In summary, TLS can be used in a multi-operator without loosing data rate compared to single-operator PF scheduling.

The following figures provide a detailed insight in the allocated data rates. Fig.

2.5 and 2.6 show the CDF of the rate allocated to 30 and 100 users, respectively. For a sharing ratio of 0.5, the TLS scheduler achieves a similar rate as the single-operator PF scheduler. However, the data rate of TLS deviates from PF in its low quantiles when unequal sharing ratios are chosen. In this case, the operator with the smaller sharing ratio (e.g. 0.25) cannot provide the high fairness among its users with respect to the operator with the larger ratio (e.g. 0.75). This results from the fact that operators with a small sharing ratio receive insufficient channel capacity to provide a high data rate at low SNR. We will detail the fairness aspect in Fig. 2.9.

The SNR distribution for the scheduled users is shown in Fig. 2.7 and 2.8 for 30 and 100 active users, respectively. Here the picture is less clear. There is no significant difference between the SNR distribution of different sharing ratios. Nonetheless, a small but significant difference between single-operator PF and TLS is shown.

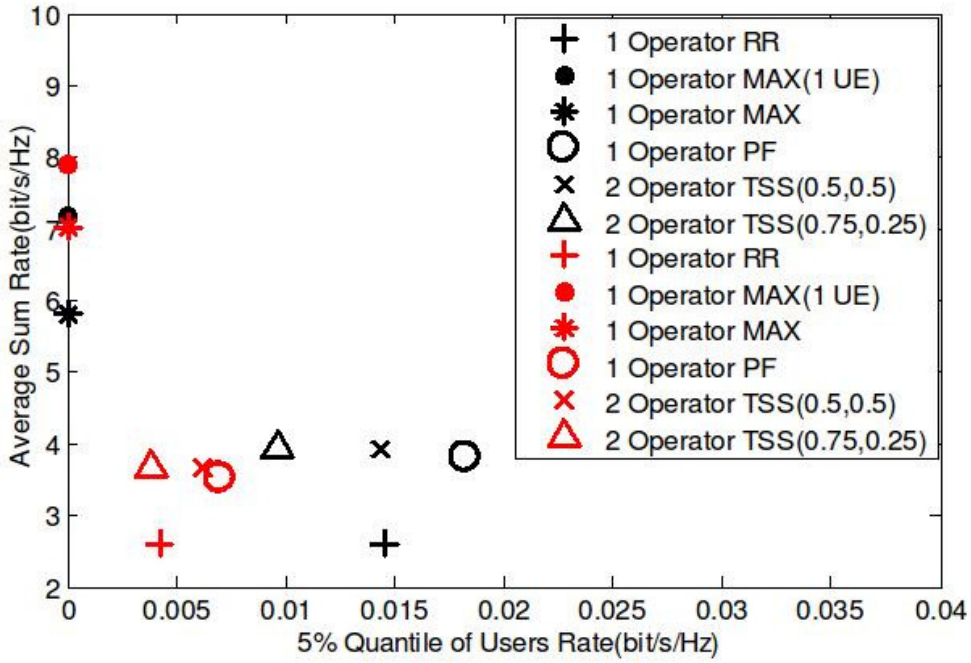


Figure 2.4: Average Sum Rate and 5% Quantile with 30 users (red values) and 100 users (black values).

To validate that TLS reaches the agreed operator sharing ratios, we study the fraction of resources allocated to the operators. The results in Table 2.2 validate that the agreed sharing ratios are achieved for 30 and 100 users.

Fig. 2.9 shows that for unequal sharing ratio among operators, the 5% Quantile of the data rate decreases. Formally speaking, when the distance between the operator sharing ratio $|g_1 - g_2|$ increases, fairness among the users decreases. This results from the fact that operators with a small sharing ratio have insufficient channel resources to keep a high data rate for users with low SNR.

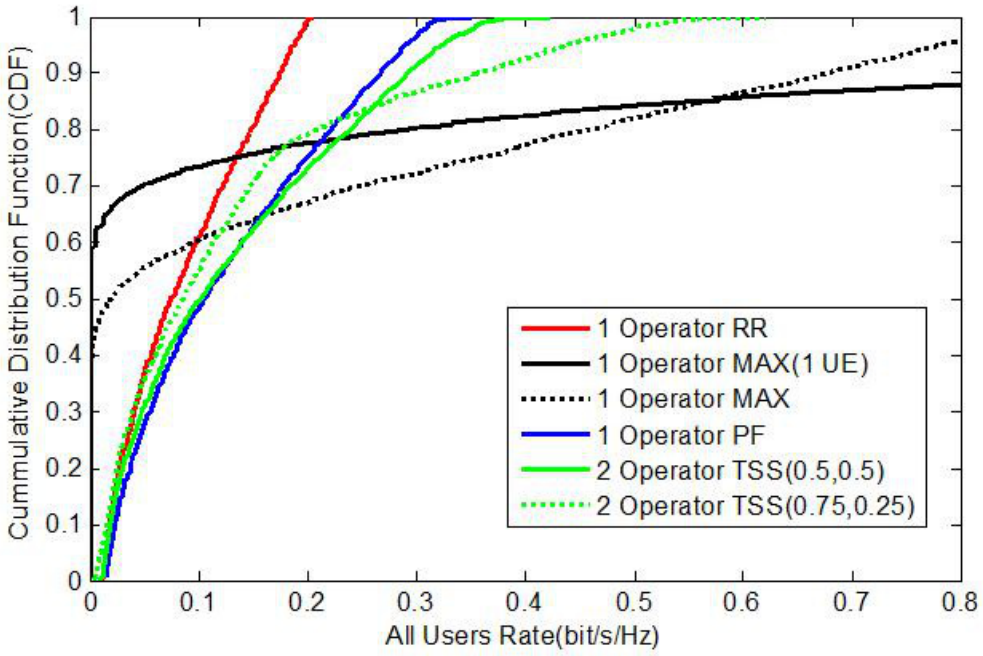


Figure 2.5: CDF of the data rate for 30 active users.

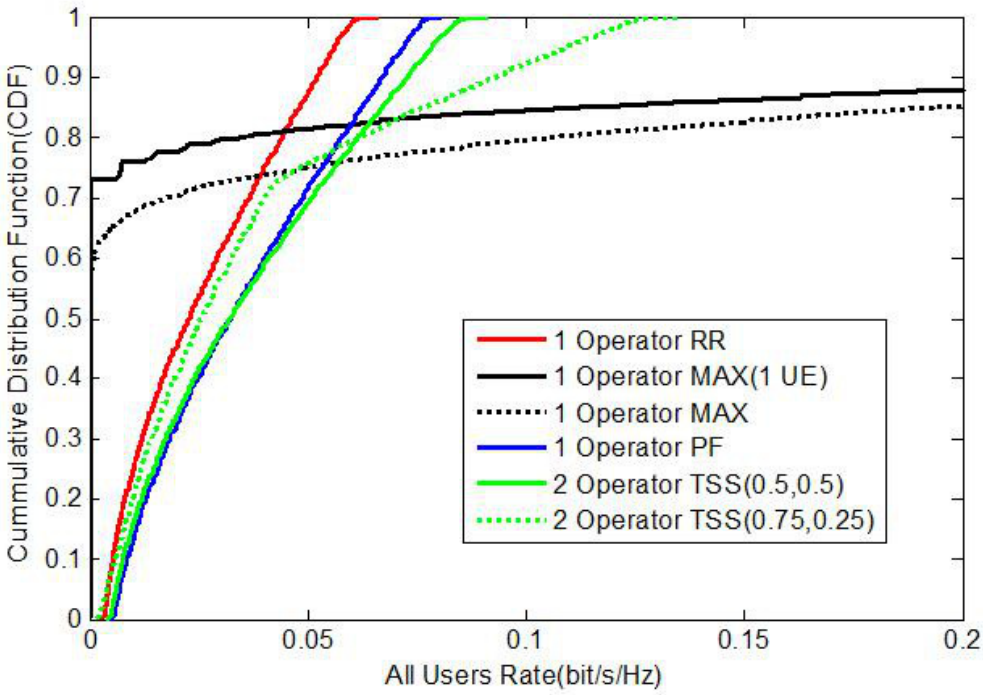


Figure 2.6: CDF of the data rate for 100 active users.

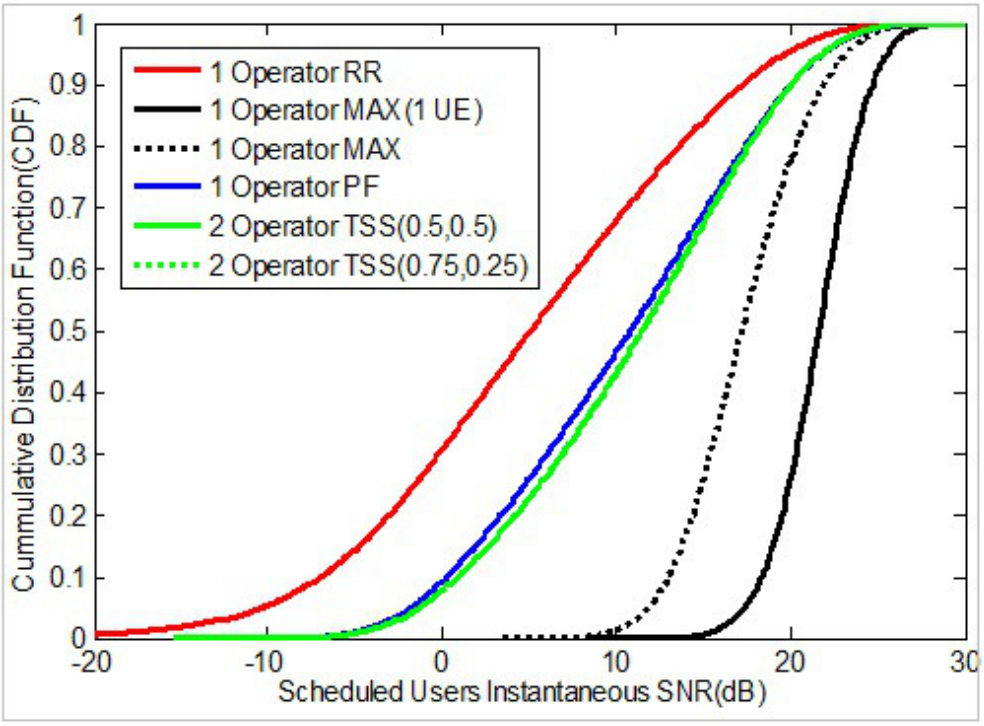


Figure 2.7: CDF of the SNR for the scheduled users, 30 active users.

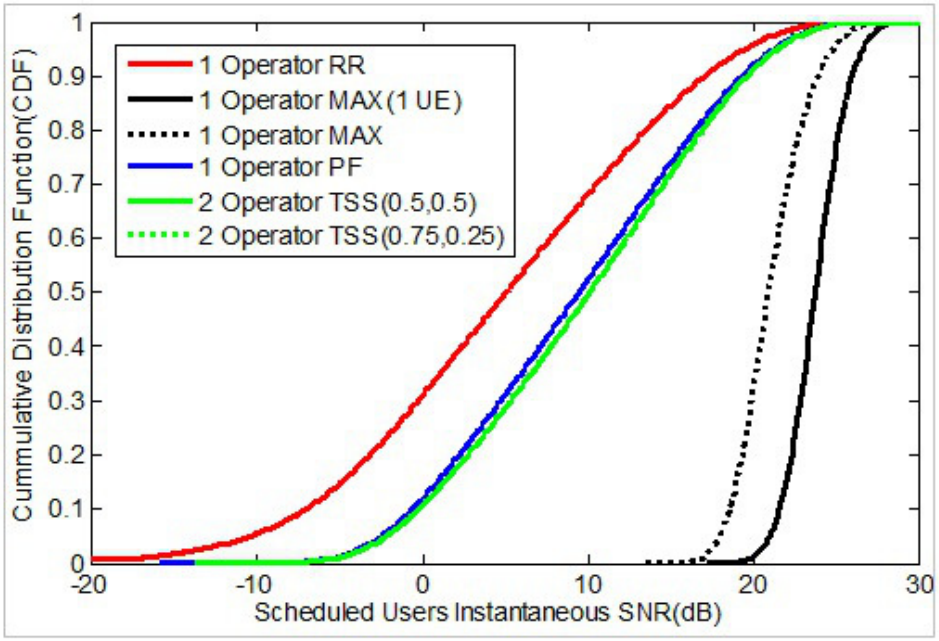


Figure 2.8: CDF of the SNR for the scheduled users, 100 active users.

## 2.7 Results of Achieved Scheduling Delay Performance

We need to study scheduling delay since TLS realizes operator sharing in time. As the scheduling delay will influence the users perception in using delay sensitive

Table 2.2: Achieved resource sharing ratios with TLS.

| | **30 Users** | **100 users** | **30 Users** | **100 users** |
|---|---|---|---|---|
| **Configured Sharing Ratio** | **operator1: 0.5 and operator2: 0.5** | | **operator1: 0.75 and operator2: 0.25** | |
| Achieved Ratio Operator 1 | 0.4983 | 0.5016 | 0.7487 | 0.7509 |
| Achieved Ratio Operator 2 | 0.5017 | 0.4984 | 0.2513 | 0.2491 |

application (e.g. gaming applications), we study the user's scheduling delay for different network loads.

For 30 active users, TLS shows no effect on the mean $\mu$ of the scheduling delay. However, the standard deviation $\sigma$ of the delay is affected by TLS. Since TLS has one further scheduling step compared to the single operator schedulers. Thus, at a sharing ratio of 0.5, TLS increases the standard deviation of the delay of single-operator PF by 1.16 ms. We refer to Table 2.3 for numerical results of the mean $\mu$ and standard deviation $\sigma$, for different scheduling policies.

Our results show that 50% of all users are served with an average delay smaller than 20 ms. This is sufficient to support even delay-sensitive applications as Voice-over-IP (VoIP). Note that, in many BS designs, this delay would be further reduced by traffic-specific prioritization, which is not considered in this paper.

Table 2.3: Achieved resource sharing ratios with TLS.

| | **Case: 30 UEs** | | | **Case: 100 UEs** | | |
|---|---|---|---|---|---|---|
| | $\mu$ | $\sigma$ | $\mu + 2\sigma$ | $\mu$ | $\sigma$ | $\mu + 2\sigma$ |
| RR | 5.00 | 0.01 | 5.02 | 16.67 | 0.48 | 17.62 |
| PF | 5.00 | 1.63 | 8.27 | 16.67 | 1.75 | 20.16 |
| TSS (0.5,0.5) | 5.00 | 2.79 | 10.57 | 16.67 | 3.42 | 23.50 |
| TSS (0.75,0.25) | 5.00 | 4.34 | 13.67 | 16.67 | 10.41 | 37.49 |

## 2.8 Concluding Remarks

We have introduced a simple Two-Layered Scheduler (TLS) for sharing wireless channel resources among the users of multiple operators. While our approach allows to execute an arbitrary multi-user scheduling policy in its second step, we studied Proportional Fair (PF) scheduling as an example. Studying the sharing ratio shows that TLS reliably allocates the resources among the operators according to the agreed shares. From studying sum rate, fairness, and delay, we can conclude that our TLS approach shows no considerable drawback compared to common single-user schedulers as PF.

Although sharing resources in time always comes at the cost of delay, the average delay is not increased and the increases in delay variance are insignificant. Overall, our simulation results demonstrate that TLS is a promising practical sharing policy.

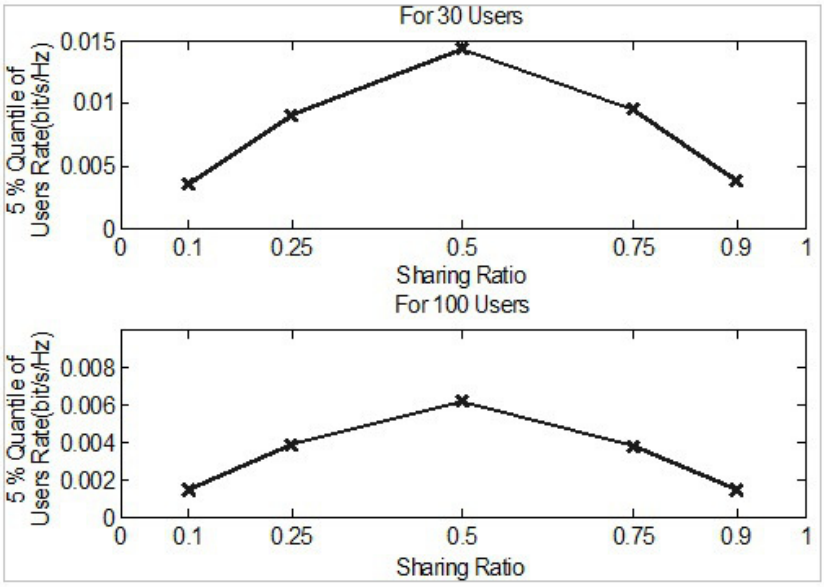


Figure 2.9: 5% Quantile of the data rate versus sharing ratio, 30 and 100 users.

# 3 Infrastructure Sharing with the Broker Based Spectrum Access

In this section, we present network sharing scenario, where two Mobile Network Operators (MNO) share the network infrastructure, while the access to the spectrum resources is under the management of the spectrum broker entity. The spectrum resources allocation scheme is based on the short-term spectrum auctioning, which is based on the game theory driven VCG mechanism; this allows dynamic allocation of the shared resources, among collocated network operators. Performance of the presented scenario has been evaluated in multicarrier High Speed Packet Access (HSPA) network, where operators are located in a multicell homogeneous grid. Spectrum usage priority among participating network operators is dynamically decided on the spectrum valuation function comparison. Moreover, the valuation functions are the input to the spectrum auctioning mechanism.

We model the cellular network radio access, considering conditional access to the shared radio resources, where the condition is based on the game theory driven principles of valuation functions. This approach provides a suitable solution for a flexible spectrum usage in cellular networks, allowing dynamic declaration of the spectrum usage rights.

## 3.1 Auctioning Mechanism

In this paper, we are skipping detailed presentation and justification of the proposed VCG based spectrum resources auctioning mechanism, providing only the reference to its description covered in earlier work [8]. Based on this mechanism, equal value, multi unit auctions in the context of radio resource allocation for cellular networks are modelled for the performance evaluation, as presented in the next section. VCG main advantages are the maximization of social value, and the incentive compatibility, which motivates the involved parties to report their true valuations for the goods being distributed.

For these purposes, we introduce a third party virtual Auctioning Unit (AU), responsible for regulating the usage and pricing of the radio resources based on valuations of those resources given by each operator. Below, we present an example of high level model of the AU unit functionality. Spectrum valuation mechanism, as well as the related discussion, is presented in [8].

## 3.2 Analytical Model

We consider two network operators, who are interested in providing services, using a particular Radio Access Technology (RAT), over the same geographical area. We assume these operators are co-located, i.e. the infrastructure sharing is used.

It is assumed that auctioning algorithm runs with the HSPA carrier granularity in the frequency domain. Time domain granularity is limited by the auction periodicity, which is considered a parameter in this analysis. The available spectrum for the auctioning game is merged into a single pool of orthogonal channels, which are available at each cell, and can potentially be used by any operator in a Time Division Multiple Access (TDMA) mode, depending on the auction outcomes in each cell. The decision of which resources are to be used by each operator for a particular time period $\Delta$ is taken by the Auctioning Unit (AU). Each AU decision is valid for a time period of duration $\Delta$, after which the Auctioning Process (AP) must be repeated and new resources allocation scheme shall be provided.

At each time interval $\Delta$, operators calculate their valuations for resources in the following time interval. Valuation information is forwarded to the cell specific AU unit. The AU decisions are based on the submitted valuations. A valuation is a function that encodes the amount of profit a particular operator expects from using a certain number of resources in the next time period. In this study, valuation is modeled on the operator specific cell load demand.

Together with the decision of who will be able to use particular resources (in this case, HSPA channel) from the auctioning pool, the AU also calculates the fees to be paid by each operator due to this usage.

## 3.3 System Model

Our system model consists of 19 3-sectorized homogeneous cells in wrap around configuration. We assume, that two MNO operators participating in the spectrum sharing auction, are co-sited, providing coverage over the same geographical area, and serve their own subscribers only (i.e. national roaming disabled). User Equipment (UE) locations are randomly generated. Assuming co-located BSs, enforcement might be seen as a limitation from the network planning perspective, but on the other hand, it opens the possibility to re-use the Radio Frequency components from the other auction player infrastructure, which might be a serious advantage in many cases. Moreover, there is the need to exchange certain amount of auctioning-related control information, i.e. BS collocation might ease practical realization of such information flow. In Table 3.1, more details on the system level model are provided.

## 3.4 Spectrum Resources Consideration

Spectrum resources allowed to be used by the AU in auctions are pooled in one set. It shall be kept in mind, that AUctioned Carriers (AUC) can be accessed by any of the auction participants, under the TDMA sharing discipline. Furthermore, licensed bands are considered for described scenarios and all auction players have equal priorities in accessing AUC carriers. We assume that each of the operators deploy Multi Carrier HSDPA network and each of them agrees to assign the number of owned HSPA carrier for the auctioning pool. Since the available channels are of

Table 3.1: Selected System Level Parameters

| **Parameter** | **Value and comment** |
|---|---|
| Network layout | Hexagonal grid, 19 sites/57 sectors, wrap around |
| Spectrum auctions setup | Auctions running in all cells |
| Inter site distance | 500 m |
| Neighbour cell modeling | Users modeled in whole network; random locations |
| Cell Isolation | 0 dB |
| UE assignment | Variable #UE/sector, per operator; default: 10/cell/op |
| Wrap around | Yes |
| Carrier frequency | 2 GHz |
| RAT | HSDPA |
| BS antenna configuration | 3 sectors |
| Antenna beamwidth | 70 deg |
| Antenna Front To Back Ratio | 20 dB |
| NodeB antenna gain | 14 dBi |
| NodeB TX power | 43 dBm |
| Power overhead for Pilot, common, shared and dedicated channels | 30% of Node B power for Primary carrier<br>20% of Node B power for Secondary carrier |
| Minimum UE to BS distance | 35 m |
| Propagation model | $128.1 + 37.6 \log 10(R)$; $R$ [km] |
| Shadow fading | 8 dB |
| Shadowing correlation | 1 between sectors, 0.5 between sites |
| Penetration loss | 0 dB - indoor scenario not considered |
| Thermal noise level | -102.9 dBm |
| Channel model | PedA 3 km/h, VehA 3 km/h |
| Fading across carriers | Uncorrelated |
| Simulation duration | Variable; default: 10 s |
| Traffic | Bursty traffic, variable burst size per operator |
| Scheduler | Proportional Fair |

identical value, the decision to be made is the number of channels to be allocated to each operator.

It is important to note that the resources sharing scenario is meaningful only in case of highly loaded networks, or in other words, in case of capacity limited networks. From practical point of view, no MNO is expected to ask for additional spectrum resources, when the currently owned spectrum resources are sufficient for smooth operation of particular network. For this reason, traffic model is seen as crucial aspect in the presented analysis due to the fact that the used valuation function is simply modelled as the cell specific data buffer size for each operator,

i.e. bids for the multi-unit auctioning purposes are modelled by the variable cell load and proportional fairness. Therefore, it is expected that the operator with highly loaded network is going to use the shared resources more frequent than the other operator.

Aspects of the equal traffic model among auction participants are investigated in [8]. Orthogonally modelled traffic arrival is proposed in [4]. Here, we evaluate HSPA system performance by considering a more realistic, partially correlated load balance among two operators, introducing tolerance on top of the reference offered cell load in order to generate operator specific load. For this purpose, tolerances of ±10% and ±50% are selected for the simulations. The smaller value simulates the sharing performance among two comparable operators. The second case is defined for less uniform market situation, e.g. MNO focusing on certain subscriber classes. Traffic model is based on the operators specific demands, being defined on the packet burst size. The number of the active subscribers using data services is fixed and constant for both operators in all sectors.

## 3.5 System Level Performance Evaluation

In this section we present and analyze simulation results, focusing on the total goodput figures for both evaluated MNOs. In Fig. 3.1 we present the allocation schemes considered in our simulations, corresponding to Scenarios 1, 2A, 2B, 3A, 3B and 3C. In the first step, we look at the throughput 50% percentile comparison for 3 scenarios, where only one carrier was released by each auction player to be pooled for sharing purposes, i.e. Scenarios 1, 2A and 3A.

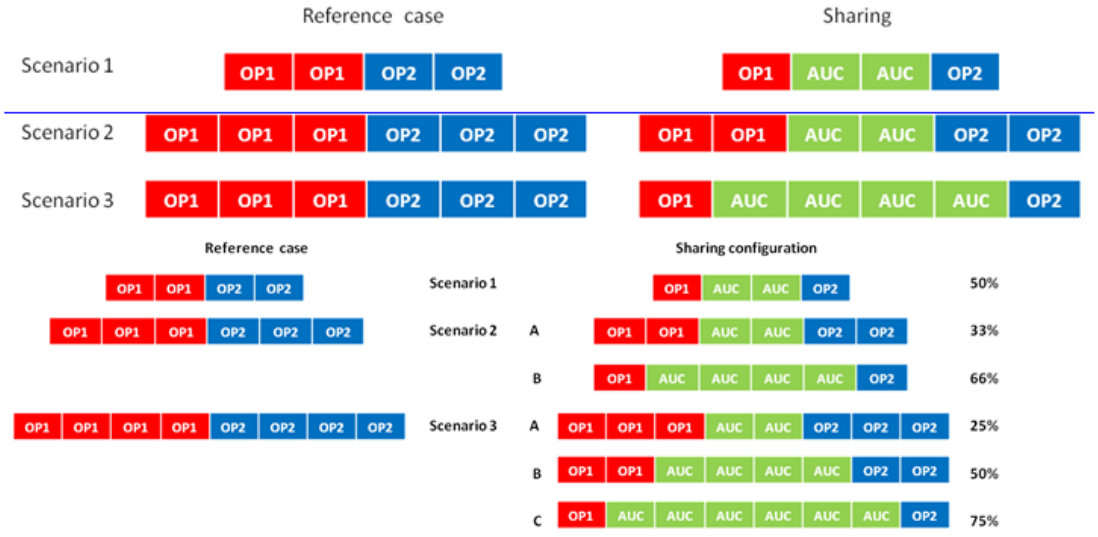


Figure 3.1: HSPA carriers allocations schemes. OP1: Operator 1 only; OP2: Operator 2 only; AUC: Auctioning Carrier - Operator 1 or Operator 2.

As depicted in Fig. 3.2, consideration of only one carrier per MNO being pooled for sharing purposes allows visible gains in terms of the total goodput, which can

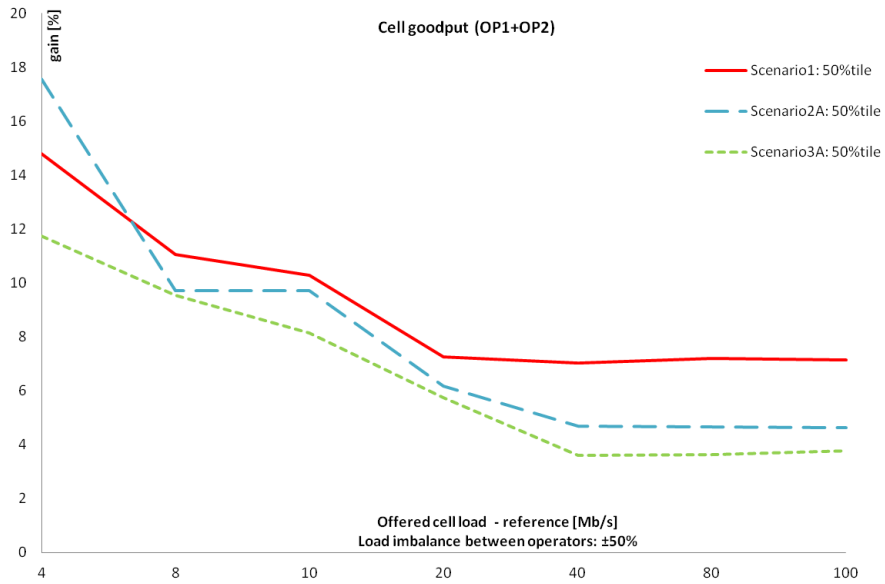


Figure 3.2: Single HSPA carrier sharing comparison, for various scenarios.

be easily translated into the increased spectrum utilization. Achieved sharing gain varies depending on the cell load and saturates for highly loaded network scenarios.

In the next step, we investigate the impact of the HSPA carrier configuration on the sharing gain over the respective reference cases, as a function of the cell load. We define two scenarios, where 50% of the owned carriers is shared by both network operators, i.e. Scenarios 1 and 3B. These configurations are selected for comparison in order to keep fixed sharing ratio as parameter. Based on the results presented in Fig. 3.3, evident sharing gains are achieved in both scenarios in terms of total spectrum utilization. It can be additionally concluded that for particular sharing percentage, i.e. 50% in this case, the cooperation results for each of the depicted throughput percentiles are reaching the saturation levels for the increasing cell load values. Furthermore, the introduced saturation levels can be considered as constant and stable. Based on this observation, the next step in the results analysis is the evaluation of the impact of sharing percentages on the total cell goodput.

In Fig. 3.4, we can observe that in the evaluated scenarios, the higher spectrum resource sharing factor is, the higher gains are achieved in terms of total cell goodput. In general, this conclusion holds for all analyzed throughput percentiles. In most cases, the highest gains are observed for 5% percentiles of the cell goodput, that can be translated into the cell edge users improvements.

Based on this observation, it would be interesting to look at larger carrier configurations, but due to the HSPA carriers spectrum requirements, higher spectrum configurations are not too realistic. Therefore, further study will be continued on the LTE network, that is out of scope of this work.

The curves depicted in Fig. 3.5 (±50% load imbalance) have non-increasing trends, which might give an impression that there are even higher gain opportunities for cell load values lower that those presented in the enclosed figures. However, a limit of these gains comes from the fact that sharing brings benefits only in case

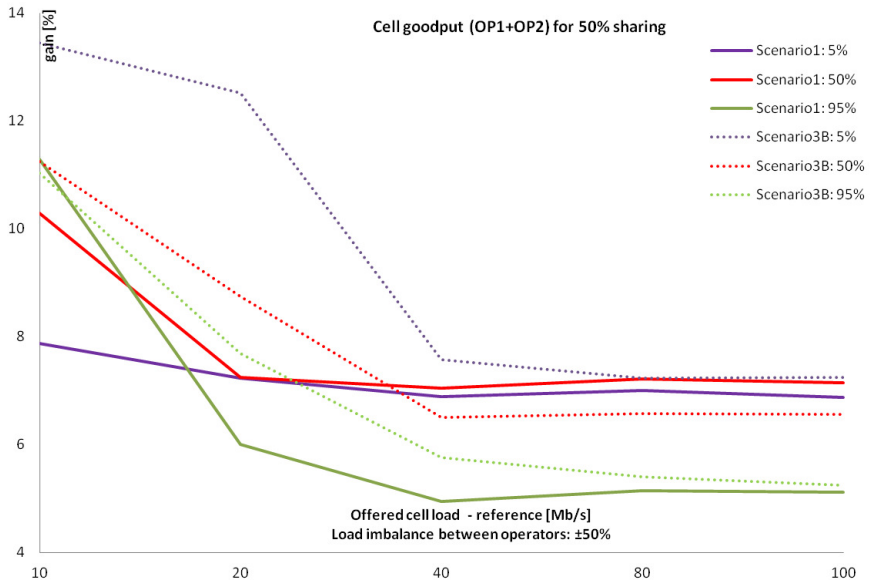


Figure 3.3: Total goodput for 50% sharing scenarios: 5%, 50% and 95% percentile comparison.

of capacity limited scenarios. Once the offered load is low enough, we do not need to participate in the described auctioning game because the exclusively owned spectrum resources are sufficient to serve the offered load. Therefore the sharing gain is no longer visible. Moreover, comparing simulation results for various load imbalance ratios between operators, i.e. $\pm 10\%$ and $\pm 50\%$, as depicted in Fig. 3.4 and Fig. 3.5, respectively, it can be noticed that the higher sharing gains are achieved in case of larger load imbalance. This can be easily explained by the fact that simple resources reuse by the network has higher load, utilizing the spectrum resources of the operator with lower valuations provided during auctions. Once the load imbalance between two networks is decreasing, the valuation functions do not allow any of the auction players to become much stronger and dominant, but as presented above, sharing gains are still clearly visible across various radio conditions.

## 3.6 Concluding Remarks

We have observed that spectrum auctioning mechanism constructed on top of the infrastructure sharing is justified in cooperation scenarios, where partially correlated and varying traffic patterns are present. The presented auction based distribution system of the spectrum resources, besides technically improving spectrum utilization, can also be seen as means to monetize the spectrum as a scarce resource.

Based on the presented spectrum utilization gains, we conclude that the described spectrum sharing algorithm extended with appropriate business model for the operators coalition formation, might bring additional money revenue gains to the network operators.

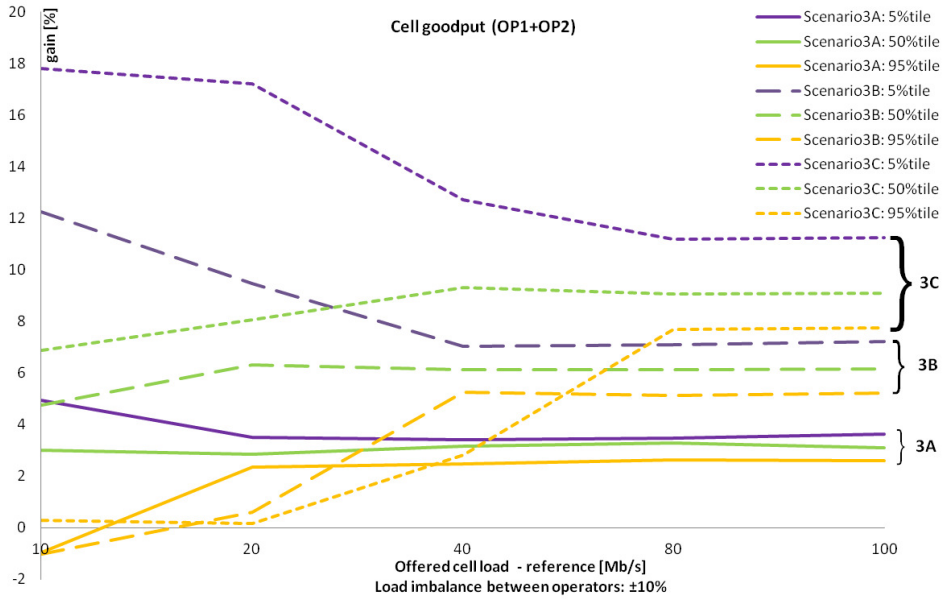


(a)

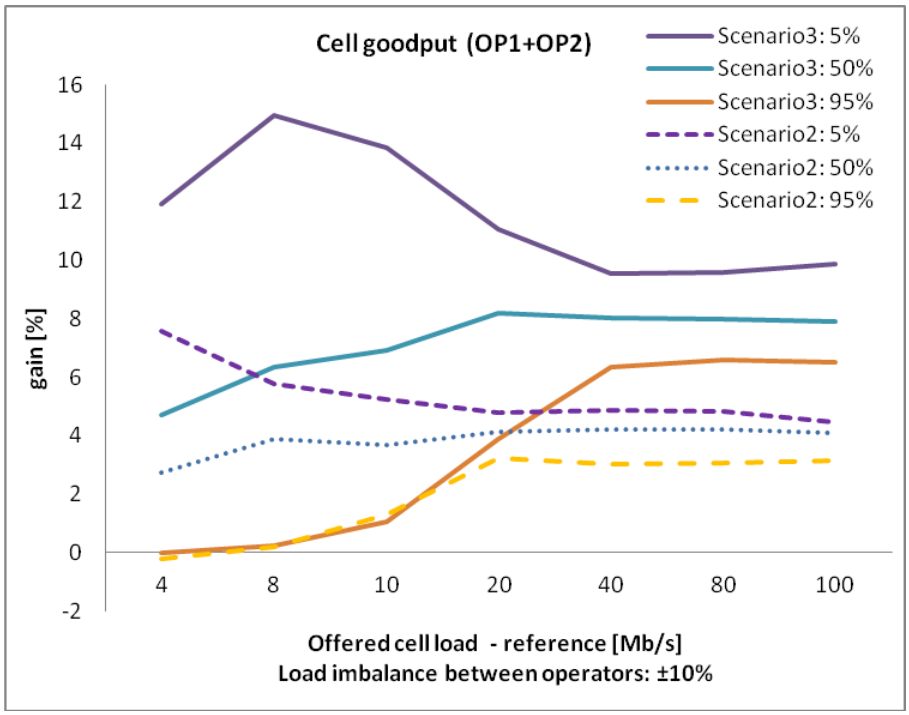


(b)

Figure 3.4: Total (OP1 + OP2) cell goodput gains: comparison of the percentiles for various spectrum sharing percentage for ±10% load imbalance.

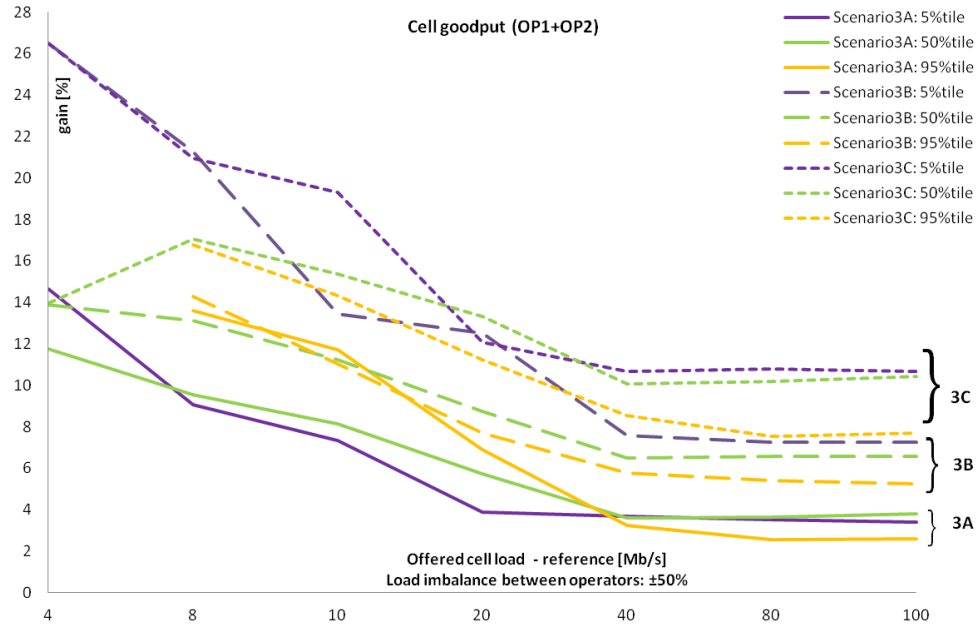


(a)

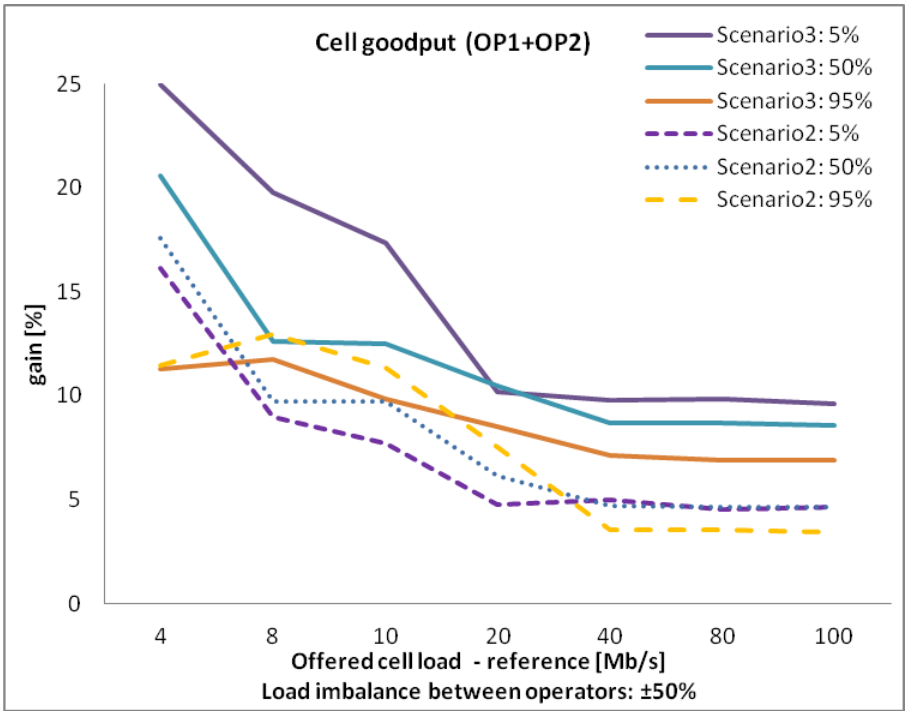


(b)

Figure 3.5: Total (OP1 + OP2) cell goodput gains: comparison of the percentiles for various spectrum sharing percentage for ±50% load imbalance.

# 4 Spectrum Sharing via Transmit Beamforming

Mobile operators are facing challenges of higher costs and carbon footprint in providing higher capacity with limited resources, including spectrum and energy. Spectrum and/or infrastructure sharing among operators is an important way to improve cost-efficiency of mobile networks.

Capitalizing on the availability of multiple antennas at the base stations (BSs), transmit beamforming techniques can be used to mitigate the interference. These techniques have been proposed to mitigate inter-cell interference in networks with aggressive frequency reuse factors; herein, we employ them to manage inter-operator interference in the case of non-orthogonal spectrum sharing. The simplest of these techniques is Zero-Forcing (ZF) which maximizes the link rate under the constraint of generating no interference to the co-channel UEs of the other operators. ZF is in general suboptimal because this constraint can be too restrictive. Performance improvement is expected by the optimal Sum-Rate (SR) technique, which however requires joint design of the BSs beamforming vectors. SR tends to favor the UE with the best channel conditions. A fairer outcome of the resource conflict arising due to spectrum sharing is the Nash Bargaining (NB) technique which distributes the rate gains due to the cooperation, taking into account the rates that the UEs would obtain without cooperation [9]. NB is also an optimal technique, since it yields one of the infinitely-many operating points on the outer boundary of the achievable rate region [10].

It is the purpose of this study to investigate how the ZF, SR, and NB beamforming techniques perform at system-level in the context of non-orthogonal spectrum sharing (also some link-level results are provided), taking into account important aspects of network operation, such as network layout, radio resource management (including packet scheduling), and dynamic traffic processing. Their system-level performance is compared with two reference scenarios: (1) orthogonal spectrum sharing and (2) fixed spectrum assignment. Further, sensitivity analysis is performed with regard to the impact on the performance of non-orthogonal spectrum sharing of (1) channel state information accuracy at transmitters (in the form of signal-to-interference-noise ratio (SINR) feedback error); (2) neighbor-cell activity level (determining inter-cell interference). We focus on downlink transmission in the study.

## 4.1 Transmit Beamforming Techniques

This section briefly introduces the transmit beamforming techniques to be investigated in this chapter.

With non-orthogonal spectrum sharing, two operators (A and B) operate on the same frequency simultaneously. Consider that $BS_1$ of operator A transmits information to $UE_1$ and $BS_2$ of operator B transmits information to $UE_2$. Assuming

that the BSs are adjacently located, both UEs receive the sum of the signals transmitted by the BSs. This setup is modeled by the interference channel. Denoting the rate for link $BS_1$-$UE_1$ and link $BS_2$-$UE_2$ as $R_1$ and $R_2$, respectively, the outer boundary of the achievable region of $R_1$ and $R_2$ is called *Pareto boundary*. It consists of the operating points for which it is impossible to improve one of the rates, without simultaneously decreasing the other [9]. For the two-user multiple-input single-output (MISO) interference channel with perfect channel state information (CSI) available at the BSs, it has been proven that any point on the Pareto boundary is achieved by beamforming vectors that are linear combinations of the ZF and maximum-ratio transmission (MRT) beamforming vectors [10]. When a BS uses the ZF (MRT) technique, it optimizes the rate of the served UE, without creating (considering the) interference to the UE of the other BS.

All the pairs of so-called Pareto-optimal beamforming vectors can be found with the computationally efficient closed-form method in [11]. Using this method, we find the SR and NB points on the Pareto boundary. The SR point maximizes the sum R1+R2, while the NB point maximizes the product $(R_1-R_1^{MRT})(R_2-R_2^{MRT})$, where $R_1^{MRT}$ and $R_2^{MRT}$ are the rates achieved when both BSs use the MRT beamforming vectors [9]. Fig. 4.1 exemplifies the positions of the SR and NB points on the Pareto boundary, for a rate region calculated using an arbitrary choice of the channel traces described in the next section. Maximum-ratio reception is used by the receivers. Fig. 4.1 also illustrates the ZF and Nash Equilibrium (NE) points achieved when the BSs use the ZF and MRT beamforming vectors, respectively. It is evident that the considered scenario is interference-limited, so that ZF is almost Pareto-optimal, whereas MRT performs unacceptably poor; hence, the performance of the latter will not be further investigated in this chapter.

In the following, we describe the key modeling aspects underlying the presented system-level performance assessment.

## 4.2 Network Layout

We consider a hexagonal layout of two co-sited sectorised LTE networks, associated with operators A and B, respectively, as depicted in Fig. 4.2. An inter-site distance of 500 meters is assumed. Each sector is equipped with four transmit antennas and has a maximum transmit power of $P_{max} = 40$ W. Each operator has a spectrum availability of 5 MHz (25 Physical Resource Blocks (PRBs)). The shaded cell is the reference cell where user sessions are generated and processed, while all neighbor cells are assumed to transmit at a fixed power of $\alpha P_{max}$, with $\alpha$ denoting the neighbor-cells activity level.

## 4.3 Propagation Environment

The radio channel traces are generated using the quasi-deterministic radio channel generator (QuaDRiGa) recently released by Fraunhofer Heinrich Hertz Institute [12]. Aiming for channel models for time evolving multiple-input multiple-output (MIMO) satellite and terrestrial cellular communications, QuaDRiGa follows the

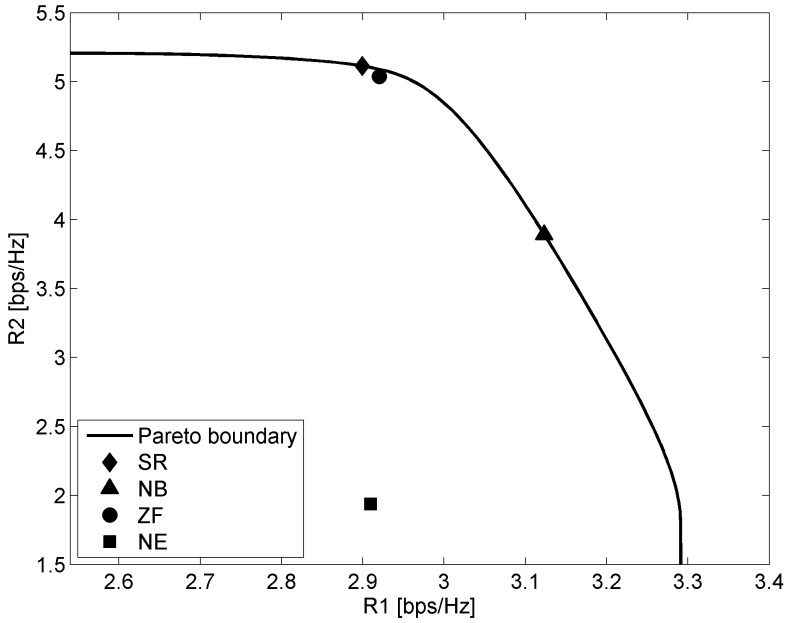


Figure 4.1: Illustration of the achievable rate region and the SR, NB, ZF and NE points, for a single realization of a UE pair at a single PRB.

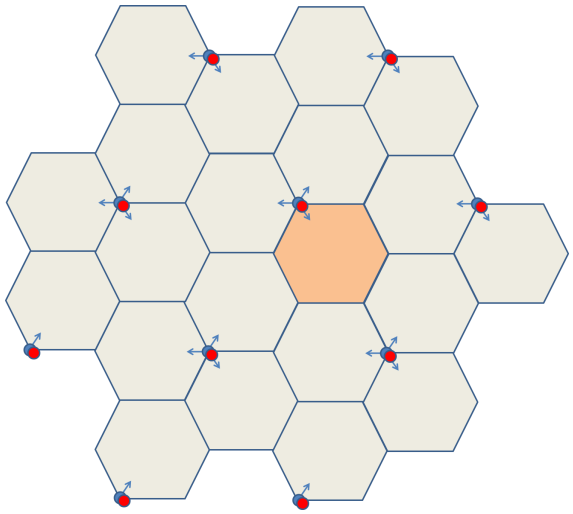

Figure 4.2: Network layout.

modeling principles of geometry based stochastic channel models like SCME, WINNER+ and the COST 2100 channel model. Interested readers may refer to [13] for the main features of the generator and channel models. For this study, the WINNER+ model is used with the major parameters summarized in Table 4.1.

Table 4.1:

| Parameter Name | Parameter Value |
|---|---|
| According to WINNER+ scenario | C2 NLOS |
| Carrier frequency (GHz) | 2.6 |
| Path loss (dB) | $35.05 \cdot \log_{10} d + 36.70$ |
| Intra / inter-site correlation | 1 / 0.5 |
| UE velocity (km/h) | 3 |
| Simulation duration (ms) | 1000 |
| Numerical independent realisation (drops) | 150 |
| Antenna pattern (eNB / UE) | KATHREIN 80010541 (10 degrees electricaldowntilt) / omnidirectional |
| Number of antennas (eNB / UE) | 4 / 2 |
| Heights (eNB / UE)(m) | 32 / 2 |
| Number of eNBs / UEs | 14 / 20 |

## 4.4 Traffic Model

User sessions are generated in the reference cell in the form of 150 independently and uniformly sampled snapshots (i.e. drops in Table 4.1) of $2 \times 10 = 20$ sessions (1 session per user), i.e. 10 sessions associated with each network (operator). For each snapshot, dynamic simulations are conducted where within each session successive file downloads are randomly and independently initiated with exponentially distributed inter-download times (with mean $\mu$) as shown in Fig. 4.3. Each download is characterized by a file size sampled from an exponential distribution with a mean of 562 kByte [14]. A file download is handled with a time-varying bit rate according to the modeled packet scheduling, link adaptation and beamforming techniques. Once all bits of a file are successfully transferred, the download is finished, its performance is administered, and the subsequent inter-download time begins until the next file download within the session is initiated.

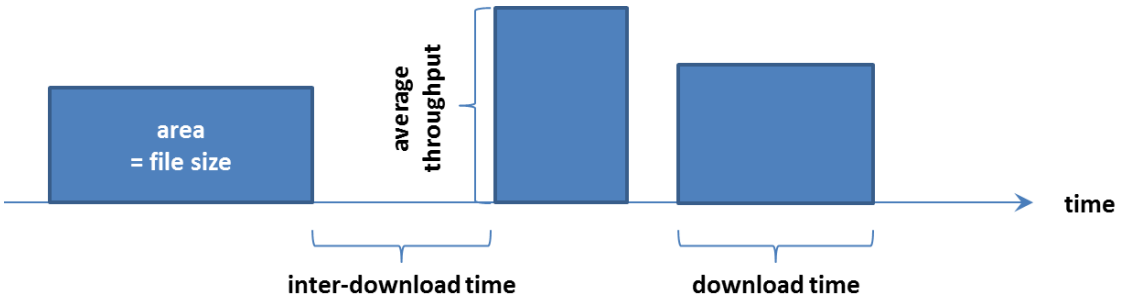


Figure 4.3: Traffic model.

## 4.5 Physical Layer Abstraction

The specifics of the propagation model, the physical layer transmission schemes and the effective interference effects are fed to the applied system-level simulator in the form of extensive sets of look-up SINR tables. These look-up tables should cover all relevant information to allow the packet scheduler to complete freely in assigning PRBs to whichever UEs are in an active session at each TTI (Transmission Time Interval), and hence also which pairs of UEs are simultaneously served at the same time in the same PRB using the transmit beamforming techniques. Specifically, for each snapshot, each beamforming technique (SR, NB, ZF), each PRB/TTI and for each pair of (potentially simultaneously served) users, a pair of SINRs is determined by stand-alone physical layer analysis and provided to the system-level simulator. In addition, a single SINR is provided to consider the case when the PRB/TTI is assigned to a single UE only (i.e. no sharing).

## 4.6 Radio Resource Management

Here we cover all system-level mechanisms employed above the physical layer abstraction to model traffic handling, i.e. EESM (exponential effective SINR mapping), AMC (adaptive modulation and coding) and packet scheduling.

EESM [15] is used to aggregate a set of PRB-specific SINRs to a single effective SINR indicating the radio link quality of a set of PRBs assigned to a given UE. EESM is characterized by MCS (modulation and coding scheme)-specific $\beta$-values, which are based on [15, 16, 17, 18].

Given a set of assigned PRBs, the AMC scheme maps the thus obtained effective SINR level to a bit rate at which the considered user is served in the given TTI. This mapping is based on the set of 15 3GPP-defined MCSs [19], the MCS-specific BLER (block error rate) curves [20], and the principle that the highest MCS is selected for which the estimated BLER is no more than 10%.

The packet scheduler is in charge of assigning PRBs to users with active downloads in each TTI. A distinction is made between three distinct network cooperation scenarios (see Section 4.7). In the case of FSA, both operators cells operate independently with a fixed availability of 5 MHz per operator, and hence scheduling is also done separately in each network. In the case of orthogonal spectrum sharing, the aggregated spectrum of 10 MHz is assigned by a "global" scheduler considering the aggregated set of active users, which implies a much greater freedom in scheduling, and hence enhanced multi-user diversity gains. Spectrum is still shared orthogonally and hence any PRB is assigned to a single user only. In the third and most complex case of non-orthogonal spectrum sharing, a similarly global packet scheduler assigns the aggregate spectrum to active users, allowing non-orthogonal spectrum sharing by assigning any given PRB to (at most) two users, employing the transmit beamforming techniques (SR, NB and ZF) discussed in Section 4.1.

In each of the cooperation scenarios, different scheduling principles can be applied. In this chapter we consider the channel-adaptive maximum sum-rate (MSR) and proportional fair (PF) scheduling disciplines. The MSR scheme, equivalent to the

commonly known "maximum SINR" scheduler, aims at optimizing cell throughput by assigning PRBs to those users with the highest sum-rate of attainable bit rates. The equally well-known PF scheme sacrifices some of this resource efficiency to establish some more user fairness by basing PRB assignments on an appropriate ratio of instantaneously achievable bit rates and an exponentially smoothed historic average of experienced bit rates. See e.g. [21, 22] for a consideration of different channel-adaptive scheduling schemes.

Acknowledging the inherently distinct fundamental objectives of the different packet schedulers (MSR, PF) and beamforming techniques (SR, NB, and ZF), appropriate combinations are considered: MSR/SR, PF/NB, MSR/ZF, and PF/ZF.

## 4.7 Research Scenarios

Based on the above discussion, we have a set of research scenarios as depicted in Fig. 4.4 These scenarios are grouped according to: firstly, the spectrum shared or assigned rule (i.e. network cooperation scenarios); secondly, the applied scheduling mechanisms; and thirdly, the applied beamforming technique (only for non-orthogonal spectrum sharing scenarios).

Since our major purpose is to investigate the system-level performance of the beamforming techniques, matched with either MSR or PF scheduling, in the context of non-orthogonal spectrum sharing (NOSS), the following scenarios could be seen as reference scenarios for performance comparison:

- Orthogonal spectrum sharing (OSS), with either MSR or PF scheduling.

- Fixed spectrum assignment (FSA), with either MSR or PF scheduling.

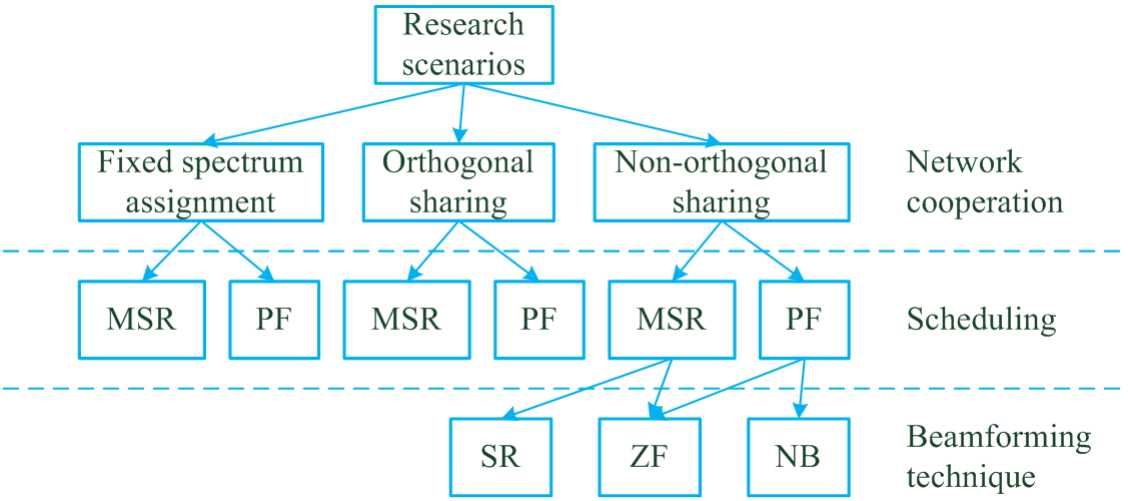


Figure 4.4: Tree of research scenarios.

## 4.8 Numerical Results and Analysis

In this section, system-level simulations are presented for the scenarios mentioned in Section 4.7 using the modeling approaches discussed in the first sections. Average user throughput, 10th percentile throughput and user fairness are major metrics used for performance assessment. User fairness is calculated using the Jain's fairness index [23]. Another relevant metric is system load (equivalent to cell throughput), which is defined as the total number of bits delivered in the system, divided by the simulation time. System load depends on the inter-download times (how much time a user spends between two successive downloads) and user throughputs (how fast a given download can be finished). Thus, even with the same inter-download times, system loads of different scenarios might differ significantly due to difference in user throughputs. Besides performance comparison among different scenarios, we also present some sensitivity analysis results showing the impact of neighbour-cell (interference) activity level and SINR feedback error. Table 4.2 shows the simulation parameter settings used in the simulations, besides those mentioned in the first sections. If not explicitly mentioned, the default settings will be used.

Table 4.2:

| **Parameter Name** | **Parameter Value** |
|---|---|
| Mean of inter-download times (s) | 0.5 (default), 10,15 |
| Neighbor-cell activity level(%) | 30,50 (default) |
| Standard deviation of SINR feedback error (dB) | 0 (default), 1, 2, 3, 4, 5 |

To better illustrate the difference between link-level and system-level performance, the link-level performance of the ZF, SR and NB techniques are first compared, for the same network configuration and parameter settings (if applicable) as the system-level simulations. The same performance metrics are used as those of system-level simulations. The difference is the way how user throughput is obtained: for each beamforming technique, each drop and each possible user pair, assuming this user pair is continuously served in each PRB and TTI, and thus the average throughput for each of the user pair can be calculated using the ways of physical layer abstraction, EESM and AMC as described in Section 4.6 (packet scheduling is not necessary). This results in totally $(10 \times 10) \times 150 \times 2 = 30000$ user throughputs.

### 4.8.1 Link-Level Results and Analysis

Fig. 4.5 shows the link-level performance of the SR, NB and ZF beamforming techniques. It is shown that the NB technique outperforms the other two techniques in the 10th percentile user throughput and user fairness, while with lower average user throughput. On the other hand, the SR technique performs closely to the much simpler ZF technique, with only slightly higher average user throughput, and slightly lower 10th percentile user throughput and user fairness. This is due to the fact that there is a relatively large number of transmit antennas and the signal-to-noise-ratio (SNR) is in general high (as observed in the CDF curves of SNR, which

are not included for brevity). Thus, inter-operator interference is the main limiting factor and it is effectively nulled with either the SR or ZF technique. This is why SR and ZF points are close in Fig. 4.1. With fewer transmit antennas and/or lower SNR, we expect larger difference between the SR, NB and ZF techniques, in the direction of the SR and NB techniques having higher average throughput and 10th percentile user throughput, respectively.

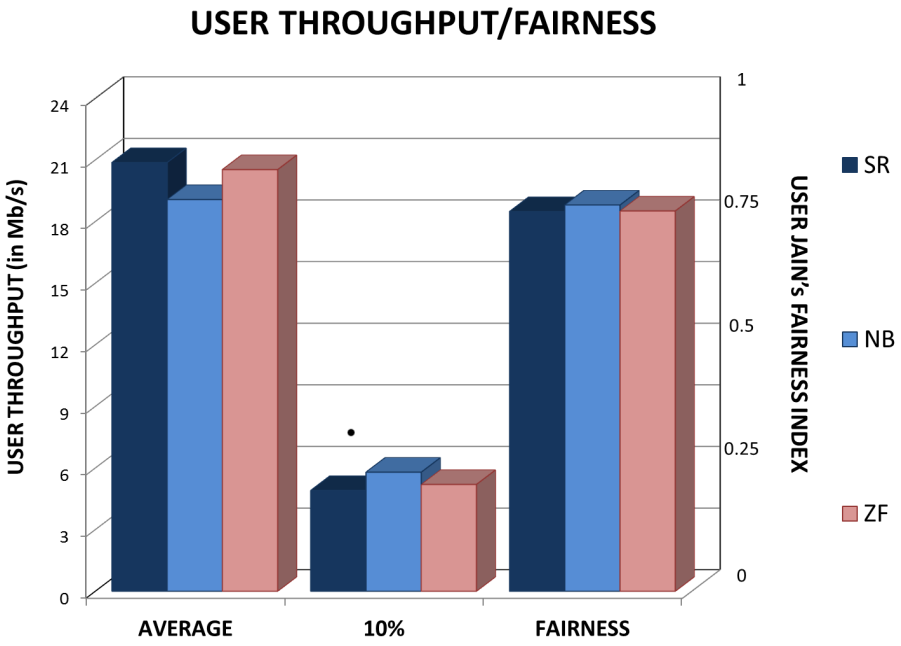


Figure 4.5: Comparison between SR, NB and ZF in link-level performance.

Fig. 4.6 shows the average throughput over distance from the BS. The maximum distance is about 330 meters, and the users are divided into 11 groups according to their individual distances from the BS (i.e. 30 meters per group). As expected, the curves are almost monotonously decreasing with the distance for all the beamforming techniques. Here, we could also see that the SR and ZF techniques perform closely, while the NB technique has lower average throughput, especially at short distance and better overall user fairness.

### 4.8.2 System-Level Results and Analysis

Fig. 4.8.2 shows the average and 10th percentile user throughput (upper), user fairness (middle) and average user throughput versus distance from the BS (bottom) of OSS and FSA, with the MSR and PF scheduling. It is shown that

- With the same scheduling method (either MSR or PF), OSS outperforms FSA in both average and 10th percentile user throughput, especially at relatively low system load. This is due to much greater freedom in scheduling and hence enhanced multi-user diversity gains in OSS than in FSA. However, such extra gains decrease with the increase of system load and distance from the BS.

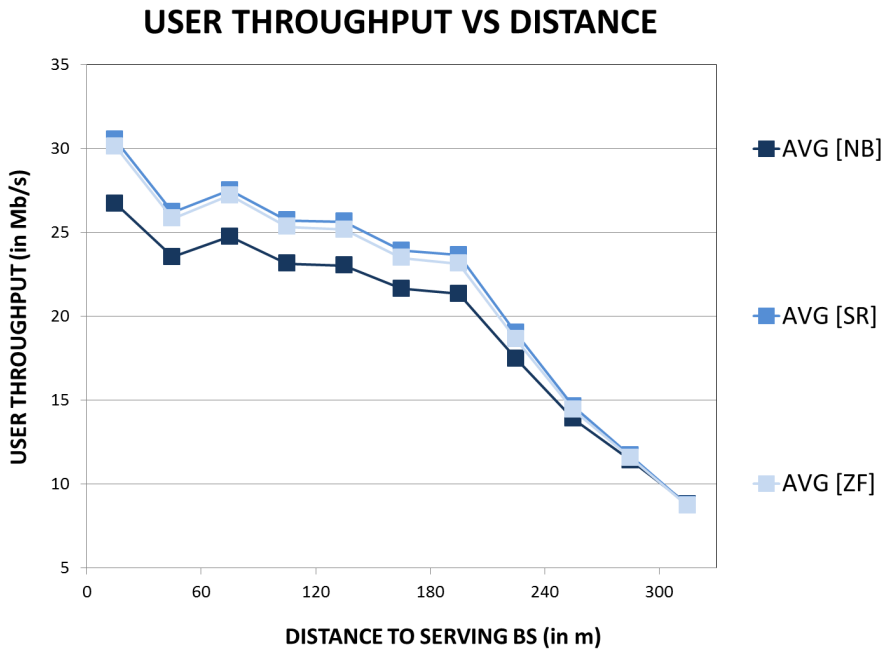


Figure 4.6: Average UE throughput versus distance (link-level).

- As expected, for the same network operation scenario (either OSS or FSA), the MSR scheduling has higher average user throughput than the PF scheduling, but lower 10th percentile user throughput and fairness.
- For the MSR scheduling, user fairness decreases with the increase of the system load. This indicates that users with good conditions still have high chance to be served at high system load, with the sacrifice of users with bad conditions.
- For the PF scheduling, user fairness generally increases with the increase of system load. This indicates that users with good conditions will be first sacrificed at high system load to stick to the fairness criteria of the PF scheduling.

Fig. 4.8.2 shows the average and 10th percentile user throughput (upper), user fairness (middle) and average user throughput versus distance from the BS (bottom) of NOSS, with 4 different combinations of scheduling and beamforming techniques: MSR/SR, MSR/ZF, PF/NB, and PF/ZF. The following remarks can be drawn.

- Although targeting at maximum sum-rate, the SR technique performs almost the same as the ZF technique, when combined with the MSR scheduling. This is due to the reason explained for the link-level analysis. Moreover, packet scheduling further mitigates the difference between the SR and ZF techniques, by selecting the most proper users for joint transmission. The latter is also in line with the analysis and conclusion of [24].
- The NB technique performs also closely to the ZF technique, when combined with the PF scheduling. This differs from the observation we have in the link-level results. This is most likely also due to the applied packet scheduling,

which mitigates the difference between the NB and ZF techniques observed in link-level performance by selecting the most proper users for joint transmission.

- Also for NOSS, the MSR scheduling has higher average user throughput than the PF scheduling, but lower 10th percentile user throughput and fairness.
- Similar to the cases of OSS and FSA, user fairness decreases with the increase of the system load for the MSR scheduling, while increasing for the PF scheduling.

Comparing Fig. 4.8.2 with Fig. 4.8.2, we could also conclude that, with the same mean value of inter-download times, NOSS outperforms OSS and FSA in average user throughput and delivered system load. However, it should be noted that the above simulation results are based on ideal conditions (i.e. channel state information is fully available at the transmitters) and a fixed neighbor-cell activity level (i.e. 50%).

Fig. 4.9 and Fig. 4.10 show some results of our sensitivity analysis, with regard to the impact of neighbour-cell (interference) activity level and SINR feedback error, respectively. Here, for the sake of simplification the SINR feedback error is modeled as random values sampled according to a Gaussian distribution with a certain standard deviation (1-5 dB). It is shown that:

- The SR technique has similar sensitivity as the ZF technique, when combined with the MSR scheduling, with regard to the impact of the neighbour-cell activity level and SINR feedback error.
- The NB technique has similar sensitivity as the ZF technique, when combined with the PF scheduling, with regard to the impact of the neighbour-cell activity level and SINR feedback error.
- As expected, a higher neighbour-cell activity level or a higher SINR feedback error will result in lower average user throughput for all the studied scenarios.

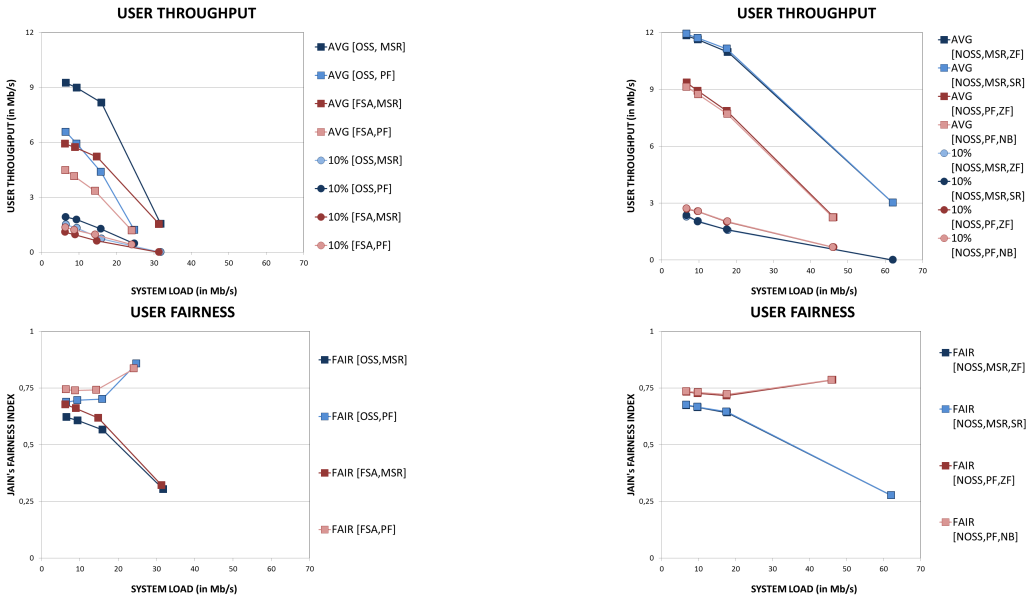

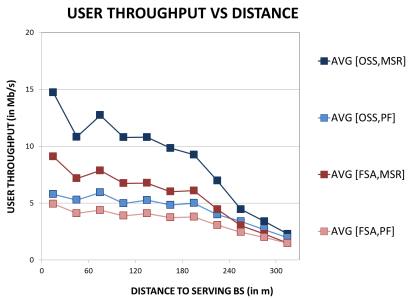


Figure 4.7: Performance of OSS and FSA: average throughput (upper), fainess index (middle) and througput vs. distance (bottom).

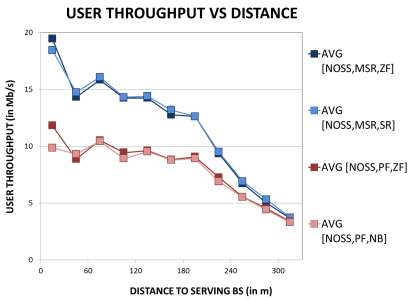


Figure 4.8: Performance of NOSS: average throughput (upper), fainess index (middle) and througput vs. distance (bottom).

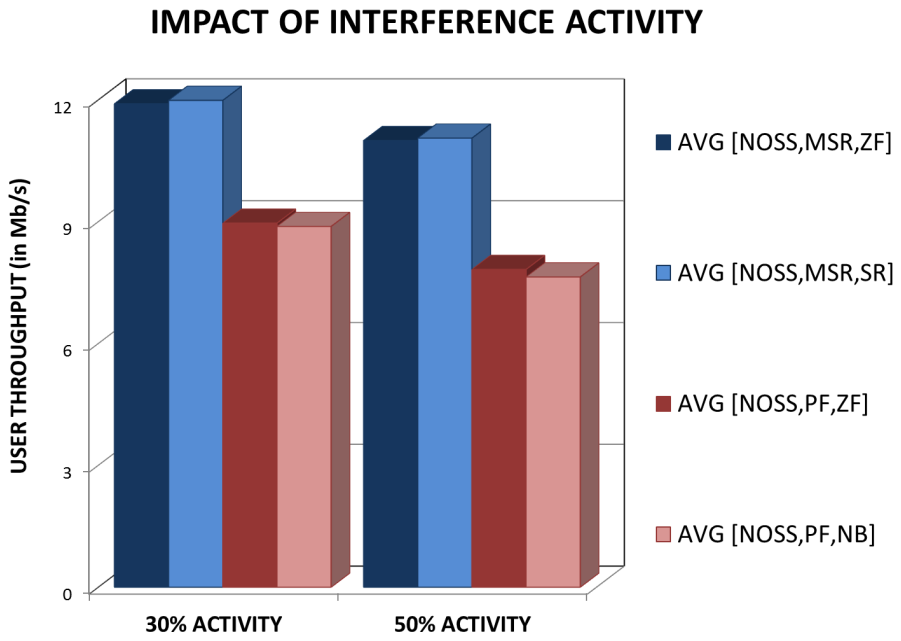


Figure 4.9: Sensitivity analysis-impact of neighbour activity level.

## 4.9 Concluding Remarks

We investigated system-level performance of non-orthogonal spectrum sharing via ZF, SR, and NB beamforming techniques. Their performance was compared with orthogonal spectrum sharing, as well as fixed spectrum assignment. For this purpose, we have proposed approaches of modeling important aspects of network operation. More specifically, an effective look-up-table based manner of physical layer abstraction has been designed to facilitate system-level simulation while meanwhile taking into account link-level difference of different beamforming techniques. Radio resource management mechanisms (including packet scheduling) have been proposed, and properly combined with beamforming techniques with the same overall objec-

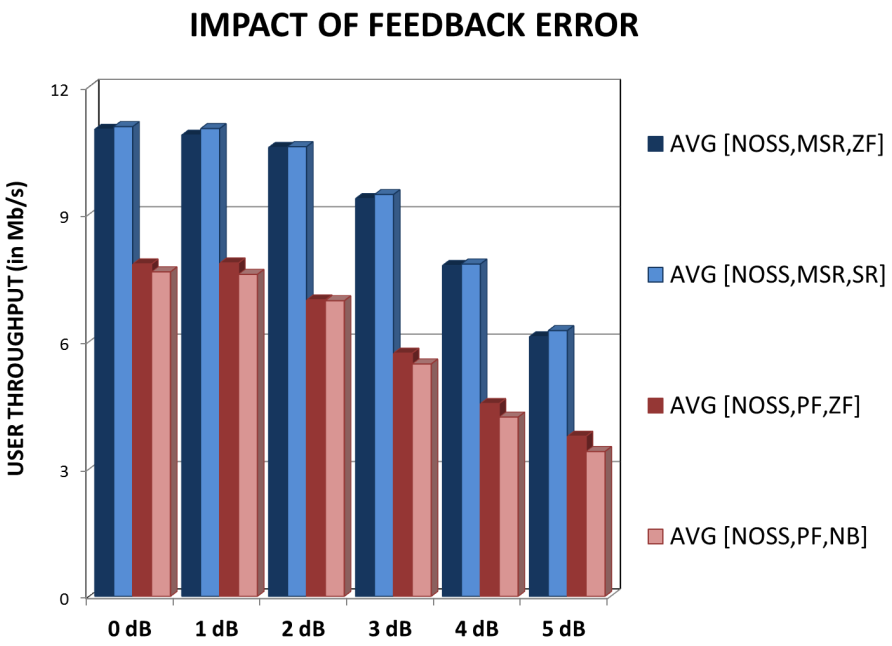


Figure 4.10: Sensitivity analysis-impact of SINR feedback error.

tives (targeting maximum sum-rate or user fairness).

The followings have been observed from the simulation results: although the SR (NB) technique outperforms slightly (significantly) the ZF technique in average user throughput (10th percentile user throughput and user fairness), such advantages of the SR and NB techniques over the ZF technique are not reflected in the system-level simulation results. This is mainly due to the fact that applied packet scheduling compensates such advantages/disadvantages, by selecting the most proper users for joint transmission. We have also observed overall advantage of non-orthogonal spectrum sharing in average user throughput and delivered system load if compared with orthogonal spectrum sharing and fixed spectrum assignment under ideal conditions.

Although in this chapter we have only shown the results of co-sited network layout, we have also performed simulations for non-co-sited cases. The results of non-co-sited cases also confirm the above observations.

Although some sensitivity analysis has been done with regard to the impact of neighbour-cell activity level and SINR feedback error on the performance of non-orthogonal spectrum sharing, it is recommended to do more sensitivity analysis with regard to the impact of other aspects (e.g. user velocity), and for other network operation as well (i.e. OSS and FSA). In our study, we have assumed at most two users sharing the same frequency (one per operator); it is also recommended to further study the case of multiple users per operator.

# 5 Beamforming-Aided Full Sharing

For fully-loaded systems, where both operators' frequency bands are fully populated, the achievable sharing gain is typically assumed to be small. This is because no operator can offer free resources to the other operator.

In this section we show that, even for such fully loaded scenarios, high sharing gains can be achieved. This is due to the following effects:

1. *Spatial diversity:* if the positions of the operator's base stations differ, then a diversity gain can be expected. For example, a user connected with operator A might be better off being served by the antennas of operator B (because of more favourable channel conditions).

2. *Beamforming:* by using multiple antennas per base station, users can be separated in space. This enables multiple users to share the same resource without excess interference.

In this section we study the gain from combined sharing and beamforming. We assume two fully loaded systems belonging to different operators. The base station antennas of both systems are at different geographical locations, as illustrated in Fig. 5.1.

For the described scenario, we are interested in the relative sharing gain resulting from spatial diversity and beamforming. By employing multiuser transmit beamforming, we are able to separate user in space, thus enabling them to share the same resource. This kind of sharing is *non-orthogonal sharing*. Although orthogonal beamforming (so-called nullsteering) is possible, we focus here on the maximum SINR strategy, since it provides the optimal trade-off between improving the SNR and reducing interference. This facilitates the co-existence of multiple operators on the same resource.

This performance gain comes at the price of creating interdependencies between the users. That is, the allocation of resources (PRBs, transmit powers) is not only limited by the power constraints imposed by the system, but also depends on the interference (or potential interference) caused to other users. This leads to coupled optimisation problems which are difficult to handle.

Within SAPHYRE, we have developed methods and algorithms for dealing with such interference-coupled problems. Firstly, we have developed non-linear interference models in WP2.3. The following algorithms and simulations are based on this model. At the core of this axiomatic framework there are the properties of "monotonicity" and "homogeneity", which are the basic features that are common to most interference functions. This makes the theory widely applicable (see Deliverable D2.3b and the book [25], which partly resulted from the research in SAPHYRE).

Monotone homogeneous interference functions are not only analytically appealing, they also offer many interesting algorithmic opportunities. In the following we will demonstrate the applicability for load balancing and throughput optimisation.

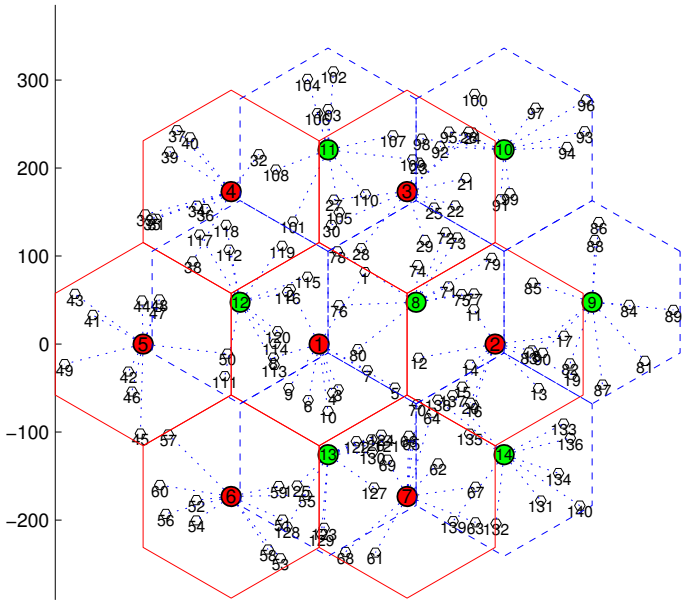


Figure 5.1: Sharing between two operators with overlapping systems

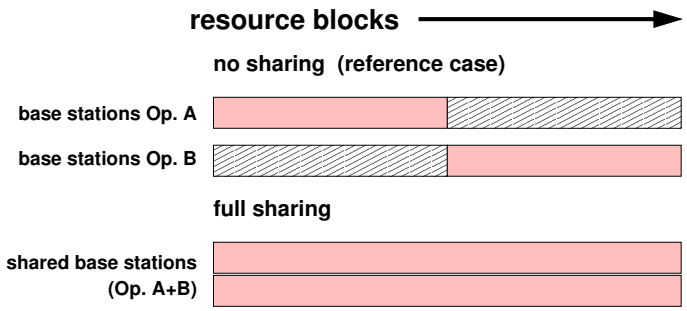


Figure 5.2: Illustration of full sharing

We assume two operators with overlapping service areas. The available spectrum (100 PRBs) is divided into two parts, as illustrated in Fig. 5.2. The downlink is considered, with parameters as described in Table 5.1. Transmission powers are allocated uniformly to the users.

Let $\boldsymbol{p} = [p_1, \ldots, p_K]^T$ be a vector collecting all transmission powers. The stochastic channels lead to spatial covariance matrices $\boldsymbol{R}_k^{(b_k)}$, which are between user $k$ and base station $b_k$ (the station to which user $k$ is assigned). The set $\mathcal{B}_l$ contains the *neighbour list* of user $l$, i.e. the list of possible candidate stations for a handover. Also, let $\boldsymbol{w}_k$ denote the $M$-dimensional complex-valued beamforming vector, where $M$ is the (variable) number of antennas at each base station, and $\|\boldsymbol{w}_k\|_2 = 1$. The vector $\boldsymbol{w}_k$ allocates the signal of user $k$ to the $M$ transmit antennas of the respective base station.

Using the duality described in Deliverable D2.3b, we obtain a "dual" uplink sys-

| | |
|---|---|
| Path-loss model | Hata-Okumura |
| Base station height: | 30m |
| Mobile station height | 1.5m |
| Channel model | 3GPP SCME |
| Frequency reuse factor | 1 |
| Cell radius | 100m |
| Power per base station | max. 46dBm |
| Carrier | 2 GHz |
| Bandwidth | max. 100 PRB/cell |
| Number of base stations | 7 per operator, 2 operators |
| User distribution | uniform random; 10 users/cell/operator = 140 |
| Beamforming | Multiuser max.SINR |
| Number of antennas | 1 at MS; variable number at BS |
| Adaptive base station assignment | proposed algorithm (min.-interference rule) |

Table 5.1: Simulation Parameters for beamforming-aided full sharing

tem, where the interference has the following structure:

$$\begin{aligned}\mathcal{I}_l(\boldsymbol{p}) &= \frac{p_l}{\max_{b_l\in\mathcal{B}_l,\ \|\boldsymbol{w}_l\|=1} \mathrm{SINR}_l(\boldsymbol{p},\boldsymbol{w}_l)} = \min_{b_l\in\mathcal{B}_l,\ \|\boldsymbol{w}_l\|=1} \frac{p_l}{\mathrm{SINR}_l(\boldsymbol{p},\boldsymbol{w}_l)} \\ &= \min_{b_l\in\mathcal{B}_l,\ \|\boldsymbol{w}_l\|_2=1} \frac{\sum_{j\neq l} p_j \boldsymbol{w}_l^H \boldsymbol{R}_j^{(b_l)} \boldsymbol{w}_l + \|\boldsymbol{w}_l\|^2\sigma_n^2}{\boldsymbol{w}_l^H \boldsymbol{R}_l^{(b_l)} \boldsymbol{w}_l} \\ &= \min_{b_l\in\mathcal{B}_l,\ \|\boldsymbol{w}_l\|_2=1} \boldsymbol{p}^T \boldsymbol{v}_{\boldsymbol{w}_l} \end{aligned} \tag{5.1}$$

with *interference coupling coefficients*

$$[\boldsymbol{v}_{\boldsymbol{w}_l}]_j = \begin{cases} \frac{\boldsymbol{w}_l^H \boldsymbol{R}_j^{(b_l)} \boldsymbol{w}_l}{\boldsymbol{w}_l^H \boldsymbol{R}_l \boldsymbol{w}_l} & 1 \le j \le K,\ j \neq l \\ \frac{\|\boldsymbol{w}_l\|^2}{\boldsymbol{w}_l^H \boldsymbol{R}_l^{(b_l)} \boldsymbol{w}_l} & j = K+1, \\ 0 & j = l\ . \end{cases}$$

This interference model contains both beamforming optimisation and adaptive base station assignment (load balancing). This enables us to take full advantage of both effects described at the beginning of this chapter: *spatial diversity* and *beamforming*.

It is observed from (5.1) that the interference is the minimum of linear interference functions, hence *monotone concave*. This property was exploited for the design of algorithms for joint resource allocation, beamforming and power control. The following optimisation goals were addressed:

- Weighted Max-Min QoS Balancing, described in the SAPHYRE publications [26, 27].
- Weighted throughput maximisation (best overall efficiency), described in the SAPHYRE publications [28, 29].

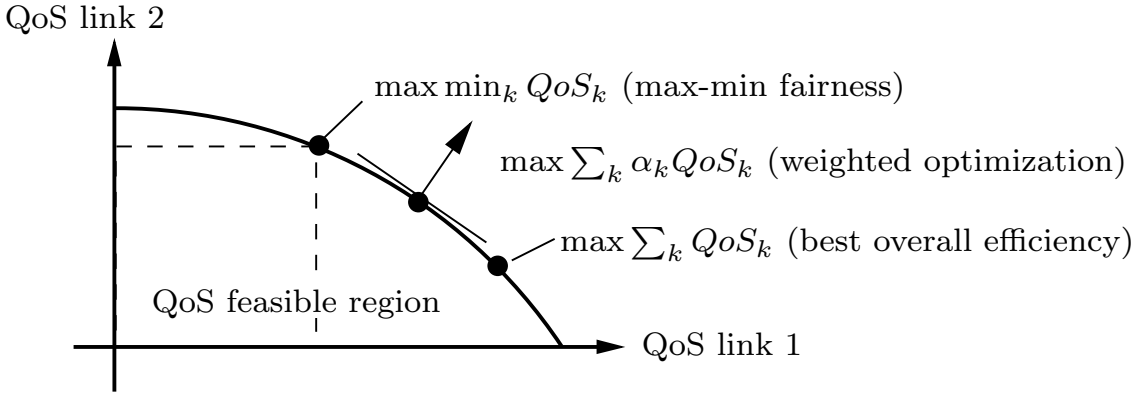


Figure 5.3: Illustration of the trade-off between fairness and efficiency

The two cases are illustrated in Fig. 5.3. Both strategies are optimal in the sense that the resulting operating points lie on the boundary of the achievable region (Pareto optimal).

Based on the interference functions (5.1), the load balancing algorithm (fixed point iteration) from [26, 27] can be used for distributing the system load more equally. This is illustrated in Fig. 5.4, where the optimised system is compared with the default scenario, where equal power allocation and a "best-SNR" base station assignment was used. It is observed that the load balancing algorithm can improve the coverage by maximising the weak users. This optimisation includes all the relevant effects: path-loss, transmission powers, and mutual interference. Those effects are all influenced by the choice of beamformers and base station assignment. The algorithm finds the globally optimal choice, as explained in [26, 27].

In order to assess the sharing gain, we want to maximise the total system throughput, where the optimisation is with respect to beamforming and base station assignment, which is included in the definition of the interference functions $\mathcal{I}_l$, as described above. The problem can be written as follows.

$$R(\boldsymbol{\alpha}) = \max_{\boldsymbol{p}\in\mathcal{P}} \sum_{l=1}^{K} \alpha_l \log\left(1 + \frac{p_l}{\mathcal{I}_l(\boldsymbol{p})}\right)$$

where $\mathcal{P}$ is the set of possible power allocations, and $K$ is the total number of users in the system. The factors $\alpha_l$ can be used to prioritise certain users. We have $\sum \alpha_l = 1$.

The problem is non-convex and even NP hard [30], thus we use the branch&bound strategy [28, 29] to compute the global optimum. This algorithm is optimal, but computationally expensive, thus only a small number of users and antennas can be simulated. The sharing gain is defined as follows.

$$\text{SharingGain} = \frac{C_{sum}(\text{full sharing})}{C_{sum}(\text{reference case})}.$$

Here, $C_{sum}$(full sharing) is the full-sharing scenario capacity, illustrated in Fig. 5.2 and described at the beginning of this chapter. Full sharing means that each operator can fully access the whole frequency band and all antennas (base stations) of

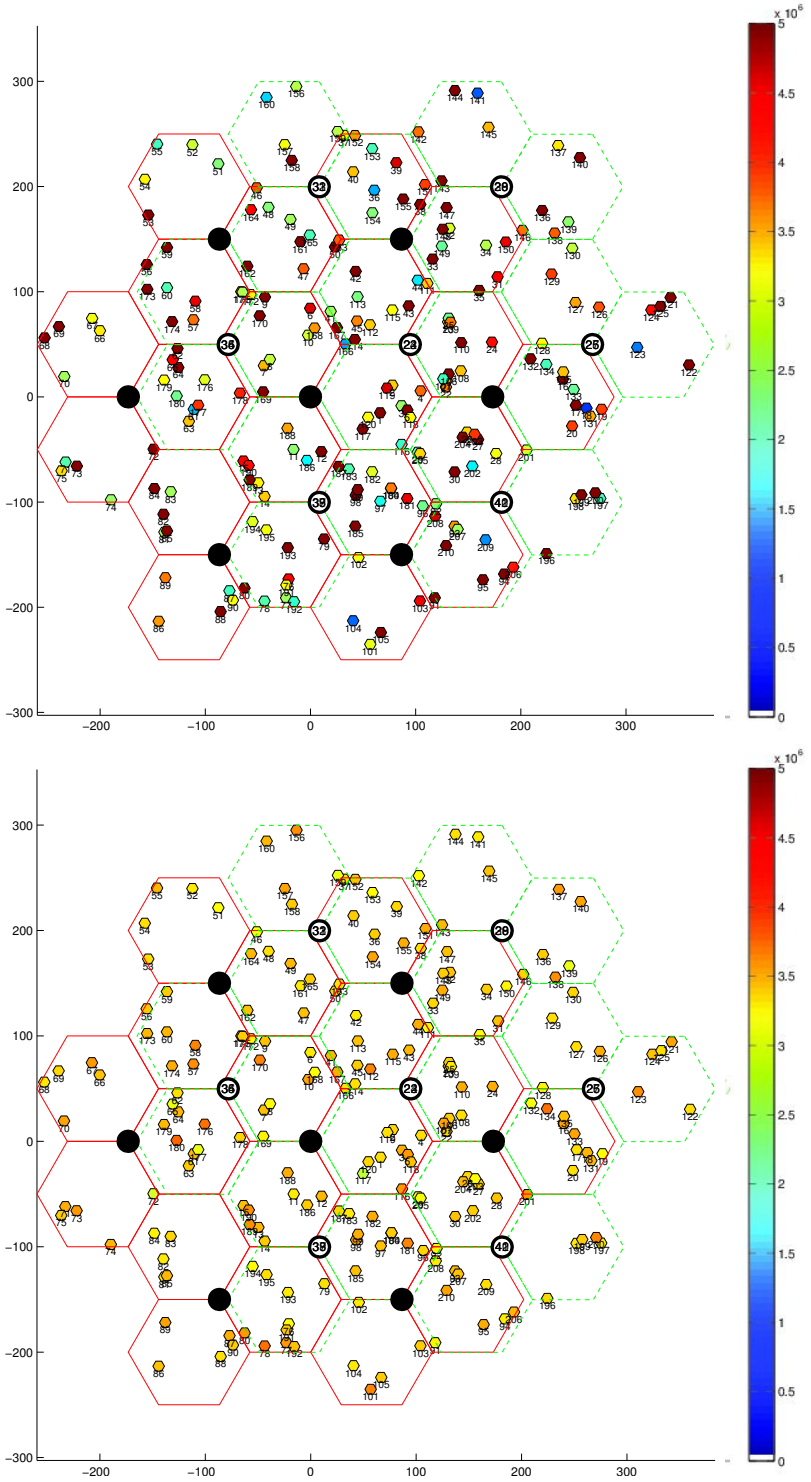

Figure 5.4: QoS Balancing for two overlapping systems with beamforming. In the figure above, the SINR distribution resulting from a uniform power allocation is shown. In the figure below, the optimised distribution, including load balancing, is shown. It is observed that the optimisation algorithm achieves a more equal distribution. This is one possible way of sharing resources.

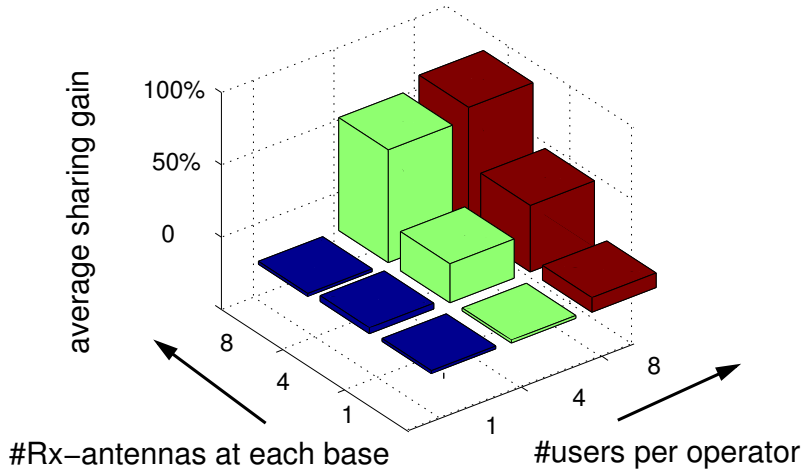


Figure 5.5: Relative sharing gain resulting from sum-throughput maximisation (branch&bound algorithm)

the system. This is compared with the reference case capacity $C_{sum}$(reference case), which uses the same optimisation algorithm with beamforming. The only difference between both scenarios is the restricted usage in terms of antennas and frequencies. For the reference case, each operator is restricted to its own antennas and frequencies, whereas for full sharing, each operator can access all available resources and antennas.

The results are displayed in Fig. 5.5. The following observations are made.

- The sharing gain is low if the number of users is small. In this case there are enough resources and there is no incentive for sharing.
- The gain is also low if the number of antennas is smaller than the number of users sharing the same resource. In this case, the algorithm has not enough degrees of freedom for separating the users in the space domain.
- Large gains up to 100% are observed for a fully loaded system with beamforming.

In conclusion, it has been demsontrated in this section that even if both operators' systems are fully loaded, a significant sharing gain is possible by exploiting *antenna diversity* (different geographical location of base stations) and *non-orthogonal resource sharing with beamforming*, which allows multiple users to co-exist on the same resource.

# 6 Spectrum Sharing Evaluation with ns3 Simulator Extension

In this section it is described a system level evaluation of the performance of the non-orthogonal spectrum sharing in a LTE scenario through the open-source network simulator NS-3 [31]. The first part presents the implementation of an extension of the Long Term Evolution (LTE) module of NS-3 that permits to simulate a MIMO 2×2 system for transmit diversity and spatial multiplexing systems. Then it is depicted an further extension of the module for the simulation of several beamforming techniques in a MISO 2×1 system. Finally, using the simulator, we evaluate the performance of the non-orthogonal spectrum sharing studying the degradation of the signal to noise ratio (SNR) in different scenarios.

## 6.1 Implementation of 2×2 MIMO in an LTE Module for the ns3 Simulator

Our developed module implements two different MIMO transmission modes: Trasmission Diversity and Open Loop Spatial Multiplexing. The former has been implemented by closely following Alamouti's precoding scheme [32], while the latter makes use of several models proposed in [33] based on different receiver designs: Zero Forcing (ZF) [34], Minimum Mean-Squared Error (MMSE) and Ordered Successive Interference Cancellation based on MMSE (OSIC-MMSE) [35].

Although we modeled two transmit and two receive antennas, the traces used for the channel can be modified for other channel models or configurations and the SINR expressions can be extended to systems with a different number of antennas, precoding schemes or receiver implementations. The module creates three new classes that are inserted within the LTE module of ns3, *MimoRxSignal*, *ScmMimoChannel* and *TransmissionMode*, described in the following subsections.

1. **MimoRxSignal**: SISO systems require the knowledge of a single channel coefficient. For MIMO systems we need a matrix **H**, modeling the channels between all possible antenna pairs. The elements of **H** are complex coefficients $h_{ij}$ representing the instantaneous gain due to fast fading from transmit antenna $j$ to receive antenna $i$.

   Class *MimoRxSignal* manages these parameters. It provides a flexible structure that includes a *MimoRx* object for every combination of a transmit and a receive antenna. *MimoRx* objects consist of four *SpectrumValue* [31] instances describing the power spectral density of the signal, the real part of the coefficient $h_{ij}$, the imaginary part of the coefficient $h_{ij}$, and the magnitude of the coefficient $h_{ij}$, respectively, in the domain of the whole LTE bandwidth.

All the instances are populated by the class *ScmMimoChannel*.

2. **ScmMimoChannel**: For the channel model, we used several traces representing the complex coefficients $h_{ij}$ for every LTE subframe, based on 3GPP SCM model[36]. The traces are generated offline by a two-step process. In the first step, a MATLAB script available at [37] is used to generate the time-domain coefficients $\eta_{ij}[n]$ with $n$ as time index. In the second step, we obtain the equivalent frequency-domain channel coefficients for every LTE Resource Block (RB) by Fast Fourier Transform. The downlink of LTE uses an Orthogonal Frequency Division Multiple Access (OFDMA) scheme, where the allocation atom is a time/frequency unit element referred to as resource block, which consists of a subchannel in frequency for a subframe in time.

   Thus, for every RB $r$ we get a matrix of coefficients

$$\mathbf{H}[r] = \begin{pmatrix} h_{11}[r] & h_{12}[r] & \dots & h_{1S}[r] \\ h_{21}[r] & h_{22}[r] & \dots & h_{2S}[r] \\ \dots & \dots & \dots & \dots \\ h_{U1}[r] & h_{U2}[r] & \dots & h_{US}[r] \end{pmatrix} \tag{6.1}$$

   where $S$ is the number of transmit antennas, $U$ the number of receive antennas and $r = 1, ..., N_{RB}$, with $N_{RB}$ being the number of resource blocks. Coefficients $h_{us}[r]$ are derived through FFT from the multipath components $\eta_{ij}[n]$, so that the variability of the gains throughout the subchannels depends on the FFT, while over time it depends on the correlation of the coefficients $\eta_{ij}[n]$'s. Such a structure realistically generalizes to a $U \times S$ matrix the current model of a SISO channel with just one coefficient.

   The channel parameters used to generate the trace inserted currently in the module are given in Table 6.1, while Fig. 6.1 shows the fast fading gain graphs obtained for two different antenna pairs in the resource-block/time domain.

3. **TransmissionMode**: The class *TransmissionMode* computes the post- processing SINR for the different implemented MIMO systems. The SINR formulas are based on [33] for a 2×2 MIMO system, with slight modifications for interference terms. for which we consider the possibility of multiple transmitters. Thus, we denote with $h_{ijk}$ the term $h_{ij}$ related to the $k$th transmitter. Also, the RB index $r$ is omitted for notational simplicity, as the procedures are simply repeated for every RB.

For the **transmission diversity** case, which corresponds to transmission mode 2 of the downlink of the LTE standard [36], we considered the Alamouti scheme [32]. The SINR expression for the $z$th receiver, under the assumption that

Table 6.1: Channel parameters.

| | |
|---|---|
| Number of antennas at the transmitter | 2 |
| Number of antennas at the receiver | 2 |
| Distance between elements at transmitter in wavelenghts | 6 |
| Distance between elements at receiver in wavelenghts | 0.4 |
| Transmitter per path Angle Spread in degrees | 2 |
| Receiver per path Angle Spread in degrees | 35 |
| Number of paths (subpaths) | 6 (20) |
| Path power in dB | [-3,...,-16] |
| Path delays in $\mu$s | [10,...,60] |
| Receiver velocity in km/h | 2 |

noise plus co-channel interference can be treated as complex Gaussian [38], is

$$SINR_z = \frac{\sum_{i=1}^{N_{rx}} \sum_{j=1}^{N_{tx}} P_{zjk} \mid h_{ijk} \mid^2}{\sigma^2 + \sum_{m \neq k} \sum_{i=1}^{N_{rx}} \sum_{j=1}^{N_{tx}} P_{zjm} \mid h_{ijm} \mid^2} \tag{6.2}$$

where $N_{rx}$ is the number of antennas at the receiver, $N_{tx}$ is the number of transmit antennas, $k$ is the index of the intended transmitter, $P_{zj\ell}$ is the power received at receiver $z$ from the $j$th antenna of transmitter $\ell$ after path and shadow fading losses, and $\sigma^2$ is a noise term. Note that the SINR formula refers to the whole receiver $z$.

Conversely, for **spatial multiplexing** we need to know the SINR value for every antenna at the receiver's side. For the ZF receiver the SINR post-processing expression for the $i$th antenna of receiver $z$ is derived as [39]

$$SINR_{z,i} = \frac{P_{zik}}{\sigma^2 \left[H_k^* H_k\right]_{ii}^{-1} + \sum_{m \neq k} \sum_{j=1}^{N_{tx}} P_{zjm} |h_{ijm}|^2 [H_k^* H_k]_{ii}^{-1}} \tag{6.3}$$

where $N_{rx} \times N_{tx}$ matrix $\mathbf{H}_k$ refers to the intended transmitter.

In the case of an **MMSE receiver**, the SINR is [33]

$$SINR_{z,i} = \underline{h_{ik}^*} R_{ik}^{-1} \underline{h_{ik}}, \quad \text{where:}$$

$$R_{ik} = \underline{h_{\ell k}} \underline{h_{\ell k}^*} + \frac{\sigma^2 + \sum_{m \neq k} \sum_{j=1}^{N_{tx}} P_{zjm} |h_{ijm}|^2}{P_{zik}} \mathbf{I}_2, \; i \neq \ell \tag{6.4}$$

where $\ell$ is the other antenna than $i$, $\mathbf{I}_2$ the 2×2 identity matrix, $\underline{h_{ik}}$ the $i$th column of $\mathbf{H}_k$, and $*$ denotes conjugate transpose.

The **OSIC-MMSE** case is an improvement of MMSE, where ordered successive interference cancellation is performed [35]. The related SINR post processing expression is obtained differently for the two antennas; first, SINR MMSE post-processing is applied for both antennas, then the substream with the highest SINR is detected and cancelled. If we denote it with $i$ then its SINR is still according to (6.4). Instead, the other substream, labeled $l$, is computed as:

$$SINR_{z,\ell} = \frac{\underline{h^*_{jk}}\underline{h_{jk}}P_{z\ell k}}{\sigma^2 + \sum_{m\neq k}^{N_{tx}}\sum_{j=1} P_{zjm}|h_{\ell jm}|^2}. \tag{6.5}$$

In all the MIMO schemes described above, perfect knowledge of the channel at the receiver is assumed.

The UML sequence diagrams reported in Figs. 6.2 and 6.3 describe the interactions between the new classes and the existing LTE modules of ns3. Fig. 6.2 represents the transmission of a signal, and shows that the new classes *ScmMimoChannel* and *MimoRxSignal* are connected to the class *SingleModelSpectrumChannel* belonging to the Spectrum Framework of ns3 through the methods of the *SpectrumPropagationLossModel* class and the *LtePropagationLossModel* class [40]. Fig. 6.3 shows instead the receiver's operation. The class *LteSpectrumPhy* separates the useful signal from interference to compute the SINR from the *LteInterference* class. Within the instance transmission mode the programmer can set, directly from the simulation script, a variable *t-mode* in order to redirect the method *ComputeSinr(..)* into the MIMO scheme of choice.

In terms of computation complexity, using MIMO schemes with the proposed approach increases the load by a factor of $N_{rx} \times N_{tx}$. Interestingly, the new classes proposed can be applied with relatively minor modifications to any other air-interfaces using OFDMA for multiple access.

## 6.2 Evalution Analysis

We ran two simulation campaigns using the approach implemented in ns3 that computes the Transport Block size considering the modulation and coding as per the standard specification [41].

In the former, we compare the simulation results with the approaches proposed in the literature to test the accuracy of our implementation. The analytical results may have limited validity in practical cases, as they necessarily neglect certain implementation aspects of the LTE standard (e.g. that the data rate is upper bounded by the highest order modulation scheme). Our simulation framework closely matches the analytical results where they are meaningful, while it generalizes them when they are no longer consistent with the system at hand (e.g. in high SINR regions).

In the latter campaign, we compare different MIMO schemes in terms of their spectral efficiency in the downlink. The purpose is to show that, even though some schemes cannot be evaluated through exact mathematical formulas, the simulator is still able to offer a quantitative comparison.

Table 6.2: Simulation parameters.

| | |
|---|---|
| Center frequency | 2.1 GHz |
| Channel Bandwidth | 5 MHz |
| Subcarrier Bandwidth | 15 kHz |
| $RB_{bandwidth}$ | 180 kHz |
| $RB_{subcarriers}$ | 12 |
| Noise figure | 5 dB |
| Noise Spectral Density | -174 dBm/Hz |
| Path loss model | COST Hata model (suburban areas) |
| BS antenna height | 32 m |
| MS antenna height | 1.5 m |
| Frame duration | 10 ms |
| TTI | 1 ms |
| Simulated interval | 25 s |

The main system parameters used in the numerical evaluations are reported in Table 6.2. Both campaigns consider a single cell scenario, therefore intercell interference is absent and SINR simply becomes SNR. This choice is not due to a limitation of the simulator, but rather to make a meaningful comparison with the past analysis. We remark that the extension to multiple cells would be straightforward in the simulator (but not in the analytical framework).

Fig. 6.4 shows the results obtained by the first simulation. The theoretical curves are given by the formula provided in [42], whose parameters have been also fitted to our scenario and the LTE standard. The value of the SNR is given by the ratio between the power at the receiver after macro and shadow fading losses and the noise value. Note that the channel model is slightly different from that considered in [42]; in spite of that, simulated and theoretical curves are similar below 35 dB, after which we obtain a saturation of the simulated curves. As argued above, this effect is due to the configuration of the LTE system which reaches at high SNRs, the most efficient modulation and coding scheme in transmission. Moreover, Fig. 6.4 shows that the performance of the ZF system is better than that of the SISO system for high SNR, and this behavior matches what expected from the theoretical analysis.

The theoretical approach used in [42] provides the performance analysis only in the cases of SISO and ZF systems. However, thanks to our module we can extend the same analysis to the transmit diversity case and to other spatial multiplexing cases. Our second simulation campaign, whose results are reported in Fig. 6.5, investigates the performance of the different MIMO schemes implemented in the module in terms of spectral efficiency. As in Fig. 6.4, the SNR considered is the ratio between the power at the receiver after macro and shadow fading losses and the noise value. An analysis of the curves related to the MIMO spatial multiplexing schemes (ZF, MMSE, OSIC-MMSE) highlights that the OSIC-MMSE receiver, thanks to the

iterative signal detection, achieves the best performance. Comparing the MIMO-MMSE curve with the MIMO-ZF curve, we notice that the MIMO-MMSE receiver provides better performance than MIMO-ZF below an SNR of 20 dB. This behavior is due to the improvement given by MMSE over ZF to reduce the impact of noise, and it is more pronounced in the region of low SNR.

Alamouti MIMO is the only diversity-based scheme included in our framework. This kind of system aims at improving the post-processing SNR at the receiver. In Fig. 6.5, we see how the Alamouti system achieves the best performance in the low SNR region. This result confirms that spatial multiplexing MIMO solutions are optimal only for high SNR (or SINR).

## 6.3 Beamforming Extension

In order to simulate the non orthogonal spectrum sharing we further extend the simulator with new functionalities that permit to evaluate the performance of linear precoding beamforming in a 2×1 MISO scenario. In the implementation we developed different beamforming techniques which include non cooperation and cooperation among the base stations. In the former we implemented the Maximum Rate Transmission (MRT) technique that maximizes the transmission rate on each link assuming that interference is absent. In this case a Nash equilibrium is achieved, and the Zero Forcing (ZF) technique permits to entirely cancel the interference created but without optimizing the useful transmission. For what concerns the cooperation beamforming, we follow the approch developed in [10] that computes the the transmit beamforming vectors that achieve Pareto-optimal points, i.e. result in data rate values for both receivers where unilateral improvement is not possible. In other words, neither receiver can get a higher data rate without the other being worse off. In particular we focused on three points of the Pareto Boundary curve: Max-Rate (MR), Proportional Fairness (PF) and Max-Min Fairness (MMF). MR selects the point that maximizes the sum rate, PF maximizes the product of the rates of the two users, while MMF maximizes the minimum of the two rates.

Fig. 6.6 shows a comparison between the theoretical capacity of the channel and the actual spectral efficiency achieved by the LTE network, computed as the ratio between the throughput and the used channel bandwidth. The throughput, in turn, depends on the Transport Block size of LTE, determined by the modulation and coding scheme, which has been computed by closely following the standard specifications [41]. Since we expect the actual spectral efficiency to be significantly lower than the theoretical capacity, these results are further compared with a heuristic estimate of the actual capacity of LTE, taken from [43]. Note that this is not a simulated value, but just a rescaling of the theoretical value, while our evaluation executes actual simulation runs. The theoretical capacity curve is verified to match the behavior identified by [11]. However, also this evaluation is now performed within the simulator ns3 and can therefore be dynamically performed for any channel realization. However, there is a significant gap between the theoretical Pareto Boundary and the actual LTE throughput. Also, the simulated values have coarser granularity (visible in the curve as fewer points in the LTE spectral efficiency curve),

which is due to quantization noise when mapping the SINR values to a finite number of Transport Block sizes, as opposed to a continuous capacity value. The figures also show the MR, PF, and MMP points along the PB curve and the projections of these points on the theoretical LTE capacity curve and on the simulated results.

## 6.4 Full Sharing Performance Evaluation

The exact characterization of the full sharing techniques in a network-wide scenario may be extremely challenging. Especially, to evaluate the resulting performance of a beamforming system involving dozens of users requires high computational power and cannot be performed in existing network simulators, unless coarse simplifications are applied on the scenario (e.g. users placed in grid-shaped formations, no mobility, and so on). In this section, we keep a more general and modular approach, which can be used in a network simulator. Therefore, we abstract all the physical layer effects by considering the Signal-to-Interference-plus-Noise Ratio (SINR) to be regulated by a parameter that we indicate as $\alpha$. This parameter depends on the mutual interference among the operators and their capability of reducing it by proper interference suppression techniques, such as efficient beamforming. The quantification of $\alpha$ influences overall metrics such as capacity, throughput, and overall QoS of the system. Thus, by giving an estimation of this parameter, the performance of non orthogonal spectrum sharing can be characterized. In particular, we will show that for scenarios where the value of the $\alpha$ parameter can be considered realistic, non orthogonal sharing leads to significant gains compared to the exclusive bandwidth allocation. In particular, these evaluations are applied to a scenario that closely follows the specification of the downlink of a LTE system, using OFDMA as the multiplexing scheme and matching all the standard specifications.

## 6.5 Adopted Scenario

The scenario of reference involves two adjacent LTE BSs managed by different operators that are serving two groups of users positioned in the same geographical region. The operators have the opportunity to share, partially or totally, their spectra. In LTE, the downlink channel of a cell is organized according to an OFDMA access scheme, which actually implies a double orthogonal division of the allocation resources over time and frequency. Time is divided into frames of 10ms, each consisting of 10 sub-frames of 1 ms. The spectrum is divided into groups of adjacent sub-carriers, and according to the portion of spectrum shared, we obtain a number of sub-channel private, i.e. used exclusively by the owner BS, and a number of shared sub-channel used cooperatively by the operators. The resources allocation scheduling depends on the type of channel, private or shared. For private channels, a policy of "max throughput" is implemented, i.e. all the resources are allocated to users who have the highest Channel Quality Indicator (CQI). Users who have not yet received a resource are sent to the shared resource pool and for each shared resource block the couple that guarantees the best rate is scheduled.

Non orthogonal sharing introduces the problem of inter-operator interference.

The signal received by each UEs is affected by the transmission toward other users that are sharing the same time-frequency resource. Then the SINR perceived by the users is degraded respect to the non-sharing case, where access to the resource is mutually exclusive and the inter-operator interference is zero. This effect can be reduced, or entirely cancelled, using the linear precoding beamforming techniques that are able to drop the interference but that in the same time decrease the useful power level received by the UEs. If $SNR_{nsh}$ is the $SNR$ in the non-sharing case and $SINR_{sh}$ is the $SINR$ in the non orthogonal sharing case, we can re-evaluate the performance of spectrum sharing scenario by considering the same indicators of the case without sharing and doing the following replacement

$$SNR_{nsh} = \frac{P_S}{\sigma^2} \implies SINR_{sh} = \frac{P_Q}{\sigma^2 + P_I} \tag{6.6}$$

where $P_S$ is the useful power in the non-sharing case, $P_Q$ is the useful power in the non orthogonal sharing case, $P_I$ the inter-operator interference and $\sigma^2$ is the noise power.

To summarize the SINR user degradation experienced in the non-sharing case, we introduce the parameter $\alpha \in (0; 1)$ defined as:

$$\alpha = \frac{SINR_{sh}}{SNR_{nsh}} \, . \tag{6.7}$$

As will be shown next, the definition of the $\alpha$ enables a compact representation of all PHY layer effects for a network evaluation, without overburdening complexity. Actually, the evaluation becomes quite flexible, as the impact of beamforming procedures and user selection mechanisms can be translated into the proper $\alpha$ value.

## 6.6 Performance Evaluation

The scenario consists of two eNBs spaced of 50m and 40 UEs for each eNBs uniformly distributed within the associated eNB coverage area. The other main system parameters are reported in Table 6.3. The sharing percentage is a tunable parameter, in a range from 0% to 100%. The $\alpha$ parameter was set from a value of $10^{-3}$ to 1, that is a sufficient range to appreciate the contribution of this parameter.

In Fig. 6.7, we evaluate how the parameter $\alpha$ affects the average throughput obtained in downlink by the base station for different percentages of sharing. As expected the value of throughput increases in the sharing cases with the value of $\alpha$. The sharing gain is obtained when the use of a larger bandwidth balances the degradation of the SINR in the MU scheme. We further explore this investigation by comparing SR and MRT in a no-sharing scenario.

Fig. 6.8 shows that, using a non-cooperative approach (MRT) among the BSs, we obtain a loss due to the increase of the interference perceived by the UEs. On the other hand, exploiting infrastructure sharing and the cooperation among the BSs through the SR approach, we can achieve a gain that permits to outperform the no-sharing scenario case. We notice that in our scenario we have only one user, so we cannot adopt any scheduling policy that permits to exploit the multi-user diversity and optimizes the beamforming algorithms.

Table 6.3: Main system parameters.

| **Parameter** | **Value** |
|---|---|
| 1-st sub-channel frequency | 2110 MHz |
| Downlink Channel Bandwidth | 5 MHz |
| Sub-Carrier Bandwidth | 15 kHz |
| Doppler Frequency | 60 Hz |
| Resource block bandwidth | 180 kHz |
| Resource block carriers | 12 |
| Resource block ofdm symbols | 7 |
| BS downlink TX power | 43 dBm |
| Noise spectral density | -174 dBm/Hz |
| Macrosopic Pathloss (distance R) | $128.1 + (37.6 \cdot \log(R))dB$ |
| Shadow fading | log-normal |
| Multipath fading | Jakes (6-12 scatterers) |
| Wall penetration loss | 10 dB |
| Frame duration | 10 ms |
| TTI (sub-frame duration) | 1 ms |
| Cell coverage | 3, 5 km |
| Cell distance | 50 m |
| Number of UEs | 40 |

These results are then compared with those provided by the first simulation, and finally summarized in Fig. 6.9 where we report the SAPHYRE gain. It can be seen how the MRT technique corresponds to a value of $\alpha$ around 0.002, while the SR technique corresponds to a value of $\alpha$ between 0.02 and 0.05.

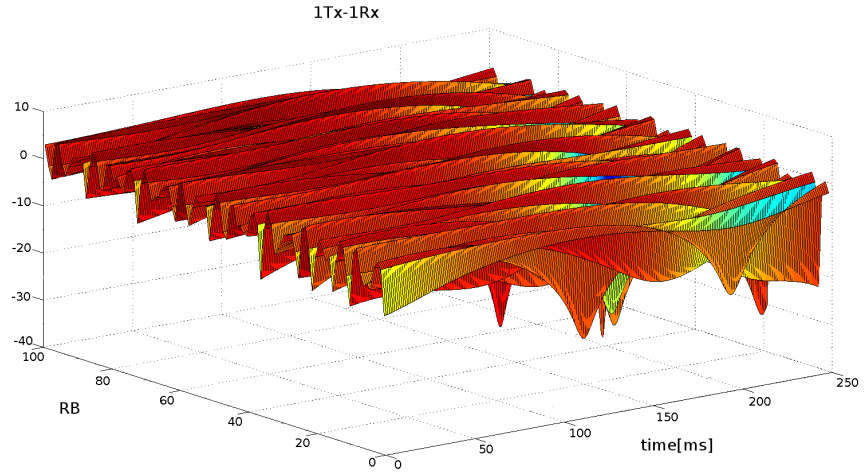


(a) Channel gain between antenna pair Tx = 1, Rx = 1.

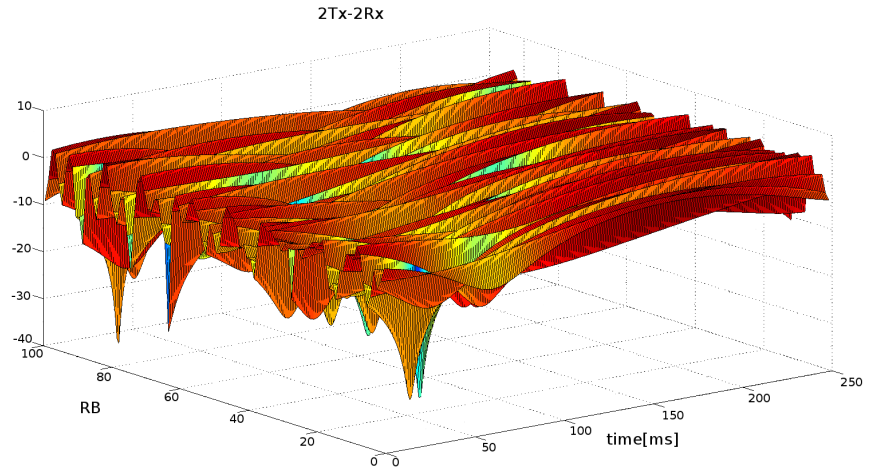


(b) Channel gain between antenna pair Tx = 2, Rx = 2.

Figure 6.1: Fast fading gain matrix for different antenna pairs.

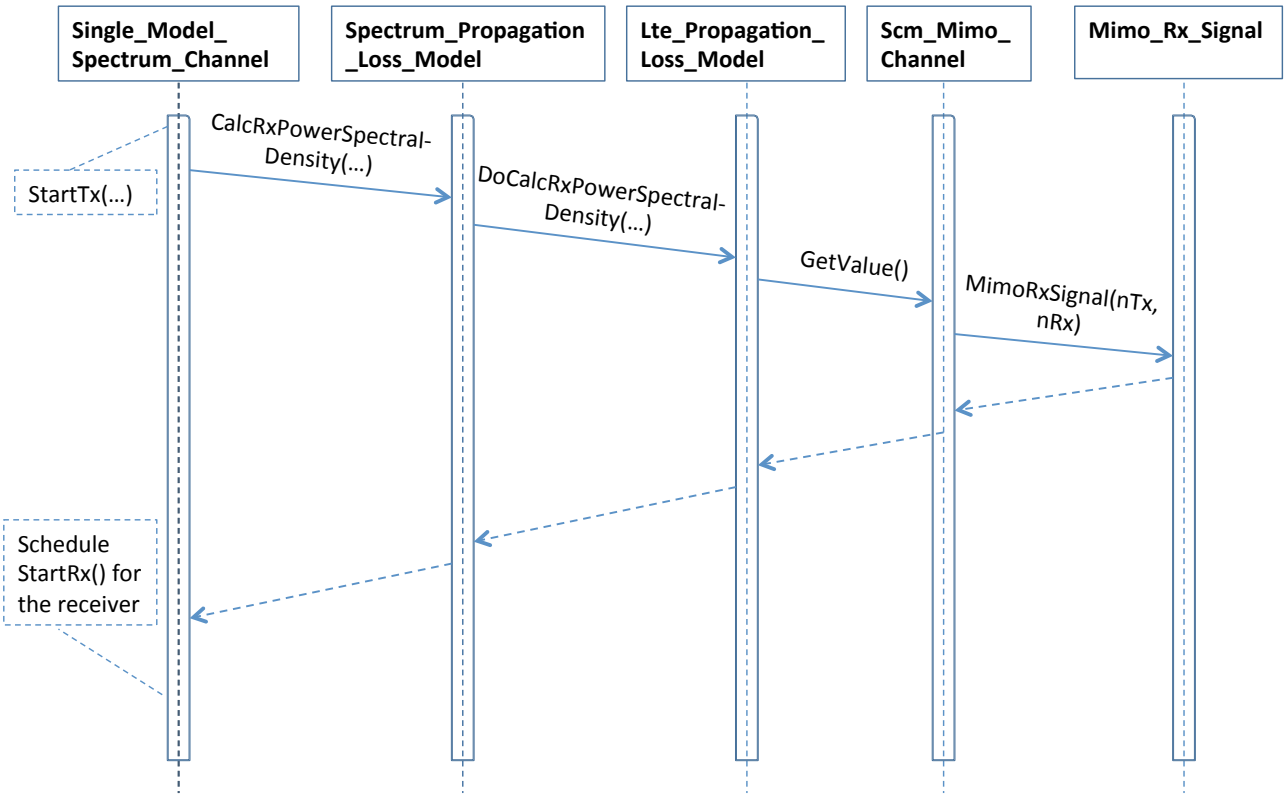


Figure 6.2: StartTx method for the transmitter.

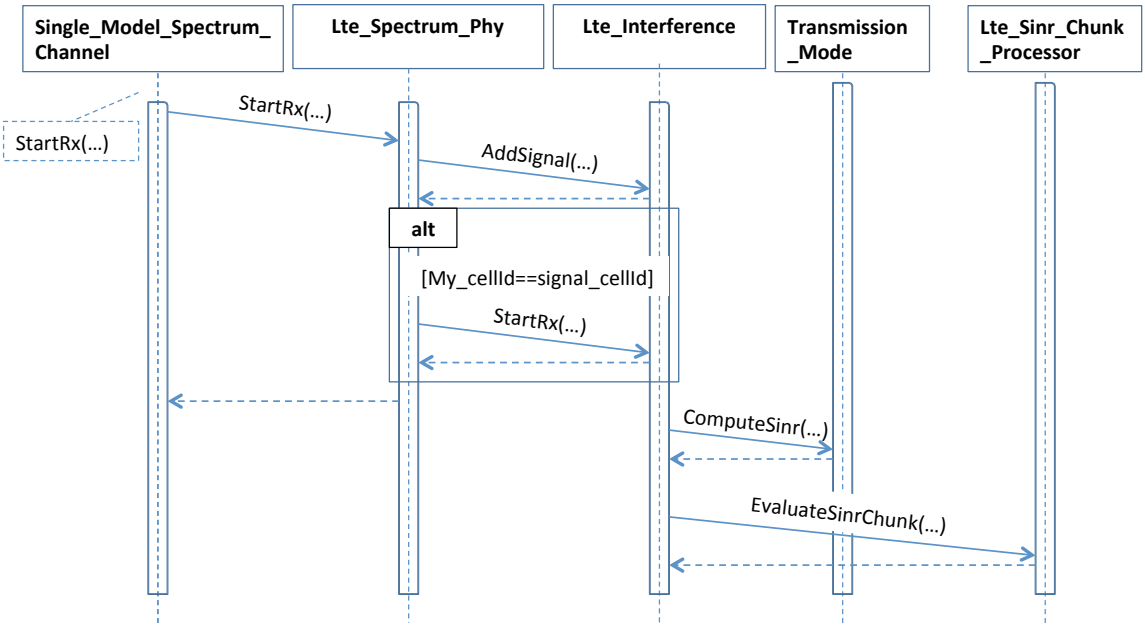


Figure 6.3: StartRx method for the receiver.

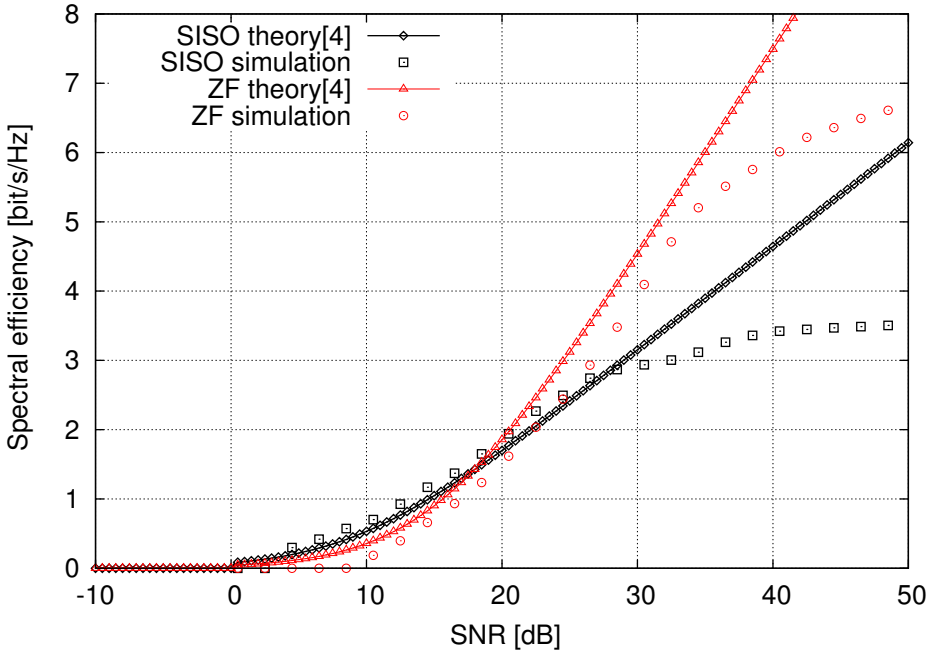


Figure 6.4: Theoretical versus simulated spectral efficiency.

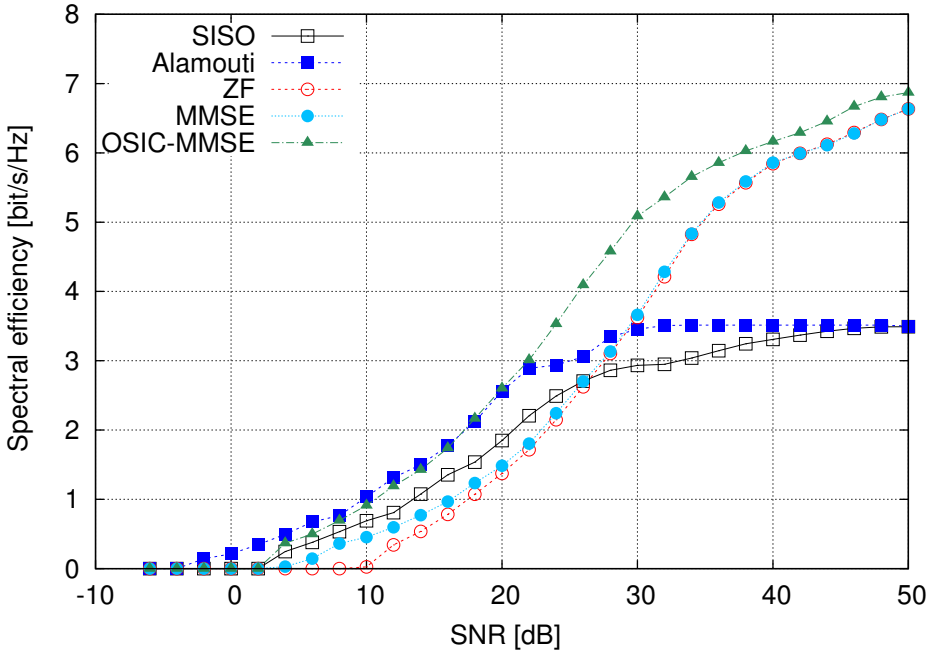


Figure 6.5: Comparison among the implemented MIMO schemes.

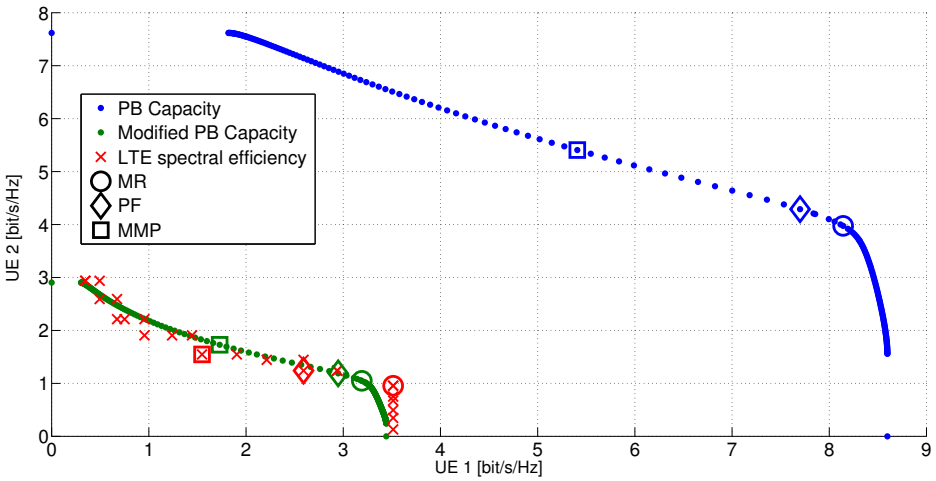


Figure 6.6: Theoretical capacity vs Simulated Spectral efficiency in a MIMO 2×1 scenario.

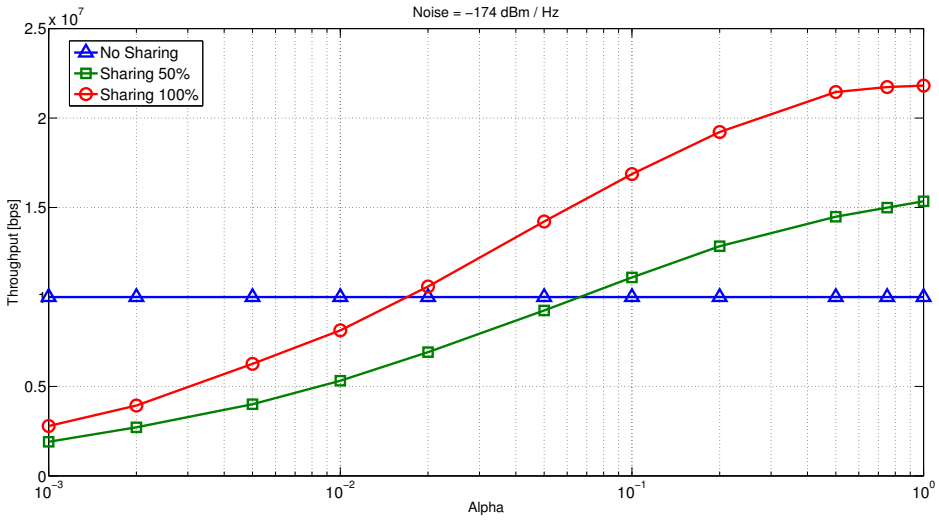


Figure 6.7: Throughput vs $\alpha$ for different percentages of sharing

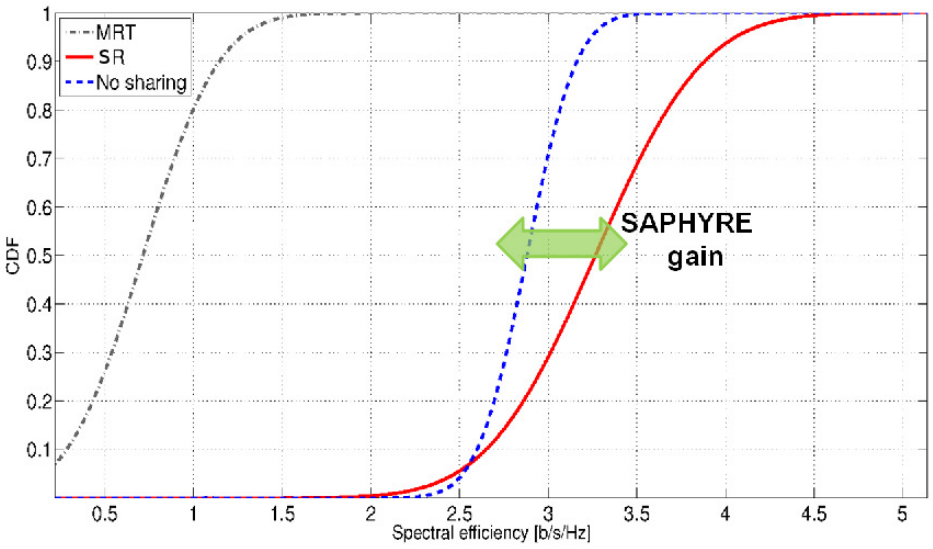


Figure 6.8: Spectrum sharing gain for different beamforming techniques

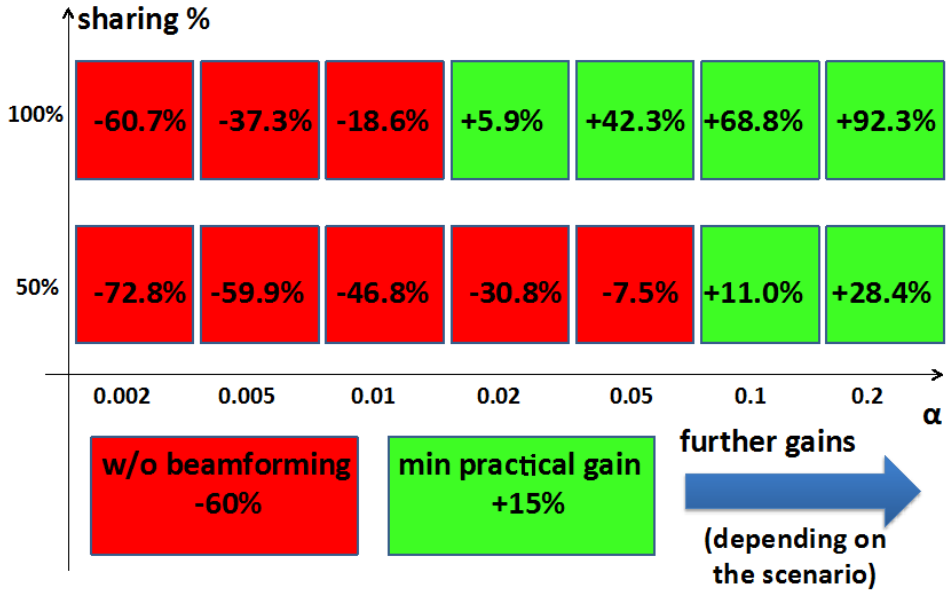


Figure 6.9: Spectrum sharing gain table.

# 7 Relay-Assisted Resource Sharing Scenario

A major challenge for future mobile communication systems beyond LTE-Advanced is to provide a wide coverage area of high data rate services as well as to increase the system capacity. An approach to achieve a wider coverage area is to increase the users throughput especially at the cell boundary by introducing intermediate nodes that act as relays. Relays which are deployed to extend the coverage of the cellular network are known as Type-1 relays [44]. The Type-1 relays have been prioritized in the LTE-Advanced Release-10 specification [45]. In SAPHYRE we study the Type-1 relays with the focus on relaying strategies (i.e. amplify-and-forward (AF), decode-and-forward (DF), hierarchical decode-and-forward (HDF)), protocols (i.e. one-way relaying and two way relaying), and the achievable SAPHYRE gain of relay assisted wireless communications.

As an alternative to DF relaying in the LTE standard [45], which decodes the desired signal and then encodes and forwards it, in SAPHYRE we investigate digital AF relaying, which exploits the advantages of MIMO techniques. One of the reasons is that compared to a DF relay, the AF relay has lower hardware requirements and results in less latency. Moreover, concerning the privacy and the competitiveness of different operators in a sharing scenario, the AF relay avoids complex signalling and data sharing among operators, e.g. an AF relay does not need the knowledge of the modulation and coding formats of different operators as opposed to a DF relay [46]. We have developed many signal processing algorithms for AF relays in Deliverables D3.1a [47] and D3.1b [48] and have demonstrated that a significant SAPHYRE gain can be achieved in link level simulations for various sharing scenarios of WP3. For example, a two-fold sharing gain in terms of the sum rate is achievable in the two-operator two-way relaying scenario in the high SNR regime and when there are many antennas at the relay [47]. The sharing gain in terms of the secrecy rate and the energy efficiency is also reported in D3.1b [48].

Nevertheless, the efficiency and usefulness of the developed algorithms in WP3 have to be verified in a system level simulation. For this purpose, we have also developed a quasi-static simulator to demonstrate the advantage of relay sharing in D4.1 and D4.3. However, on the one hand, the developed simulator is simplified and can only demonstrate limited system level performance of relay sharing scenarios. On the other hand, even the system level simulation of non-sharing scenarios with relays is inherently difficult to implement. Unlike the traditional cellular networks, there are no common agreements regarding the hardware configuration of relays, e.g. transmit power, sectors, etc. The layout of such a cellular network is also unclear since the recommended number of relays per sector/cell and the recommended position of relays is still under investigation. The theoretical research on limits of relays is also undergoing. Although there are some system level simulation results reported in [49] and [50], they are based on a simplified model as well. Due to the aforementioned problems, the system level simulation for demonstrating the sharing

gain of relay sharing scenarios in the SAPHYRE project is not presented in this deliverable. For readers who are interested in algorithms and the testbed demonstration for relay assisted resource sharing can refer to D3.1a [47], D3.1b [48], and D6.3b [51].

# 8 Conclusions

This deliverable reviewed and evaluated resource sharing paradigms from a system level perspective in different scenarios involving next generation wireless networks. From all the reported evaluations, the main conclusions can be summarized as follows.

First of all, spectrum sharing is envisioned as a promising technique to improve system capacity of wireless network at different levels. Especially, our evaluations propose *non-orthogonal* spectrum sharing as achieving a SAPHYRE gain in system capacity which is above 15%, which appears to be a worst-case value. Moreover, much higher gains can be obtained in different scenarios, depending on asymmetries between the operators and traffic patterns, as was already the case for orthogonal sharing. However, non-orthogonal sharing is also able to achieve inherent gains due to increased frequency diversity. Therefore, it is reasonable to expect such a technique to allow significant performance enhancement in practical cases.

Moreover, we also evaluated other kinds of resource sharing paradigms, including infrastructure and relay sharing, and also full resource sharing. We envision the resulting sharing approaches as possible candidates for the operation policies of next generation network operators.

Finally, our evaluations also show that advanced wireless communication techniques are needed to achieve the gains of resource sharing. In particular, beamforming stands out as the strongest enabler of SAPHYRE gains. Additionally, we assessed that, in order to achieve these gains from a system level point of view, no major modifications, but only proper management, of existing physical layer techniques is required.

Therefore, these results show a cross-fertilization of research areas in that performance improvements brought by physical layer techniques can be extended, if properly managed, up to the network layers as well, while at the same time these promising results obtained by system level evaluations may reinforce and open up new research directions in the field of physical layer techniques.

# Bibliography


[1] *Network Sharing in LTE – Opportunity & Solutions*, Alcatel-Lucent, Resource Center, 2010.

[2] T. Frisanco, P. Tafertshofer, P. Lurin, and R. Ang, "Infrastructure sharing and shared operations for mobile network operators from a deployment and operations view," in *Proceedings of the IEEE Network Operations and Management Symposium*, 2008.

[3] G. Salami, A. U. Quddus, D. Thilakawardana, and R. Tafazolli, "Nonpool based spectrum sharing for two umts operators in the umts extension band," in *Proceedings of the IEEE International Symposium on Personal, Indoor and Mobile Radio Communications (PIMRC)*, 2008.

[4] R. Litjens and H. Zhang, "Analytical assessment of the performance impact of spectrum sharing in cellular networks considering different time scales," in *Proceedings of the European Signal Processing Conference (EUSIPCO)*, 2011.

[5] J. Lee, J. G. Andrews, and D. Hong, "The effect of interference cancellation on spectrum-sharing transmission capacity," in *Proceedings of the IEEE International Conference on Communications (ICC)*, 2011.

[6] Q. H. Spencer, A. Swindlehurst, and M. Haardt, "Zero-forcing methods for downlink spatial multiplexing in multiuser MIMO channels," *IEEE Transactions on Signal Processing*, vol. 52, no. 2, pp. 461–471, 2004.

[7] O. Aydin, W. Jamil, and S. Valentin, "A two-step scheduler for the dynamic sharing of wireless channel resources among operators," in *Proceedings of the IEEE Vehicular Technology Conference (VTC)*, 2013.

[8] T. Fahldieck, M. Szydełko, H. Zhang, M. Schubert, L. Anchora, and J. Zhang, "Resource allocation and interference management strategies," SAPHYRE Project FP7-ICT-248001, Deliverable D4.1, 2012.

[9] E. G. Larsson, E. A. Jorswieck, J. Lindblom, and R. Mochaourab, "Game theory and the flat-fading gaussian interference channel," *IEEE Signal Processing Magazine*, vol. 26, no. 5, pp. 18–27, 2009.

[10] E. A. Jorswieck, E. G. Larsson, and D. Danev, "Complete characterization of the Pareto boundary for the MISO interference channel," *IEEE Transactions on Signal Processing*, vol. 56, no. 10, pp. 5292–5296, 2008.

[11] J. Lindblom, E. Karipidis, and E. G. Larsson, "Closed-form parameterization of the Pareto boundary for the two-user MISO interference channel," in *Proceedings of the IEEE International Conference on Acoustics Speech and Signal Processing (ICASSP)*, 2011.

[12] *QUAsi Deterministic RadIo channel GenerAtor (QuaDRiGa)*, Fraunhofer-Gesellschaft, Heinrich-Hertz-Institut, 2012, [Online] *http://quadriga.channel-model.de/*.

[13] K. Borner, J. Dommel, S. Jaeckel, and L. Thiele, "On the requirements for quasi-deterministic radio channel models for heterogeneous networks," in *International Symposium on Signals, Systems, and Electronics (ISSSE)*, 2012.

[14] "Http archive, mobile web performance data (iphone), [online] *http://httparchive.org, 2012.*"

[15] *System-level evaluation of OFDM – further considerations*, TR r1-031303 ed., Ericsson, 3GPP, 2003.

[16] *Feasibility study for Orthogonal Frequency Division Multiplexing (OFMD) for UTRAN enhancement*, TR 25.892 ed., 3GPP, 2004.

[17] M. Doettling, "Assessment of advanced beamforming and MIMO technologies," WINNER Project TR IST-2003-507581, Deliverable D2.7, 2005.

[18] D. Huy, R. Legouable, D. Ktenas, L. Brunel, and M. Assaad, "Downlink B3G MIMO OFDMA link and system level performance," in *Proceedings of the IEEE Vehicular Technology Conference (VTC)*, 2008.

[19] S. Sesia, I. Toufik, and M. Baker, *LTE: The UMTS Long Term Evolution: From Theory to Practice*. Wiley&Sons, 2009.

[20] C. Mehlführer, M. Wrulich, J. C. Ikuno, and D. Bosanska, "Simulating the long term evolution physical layer," in *Proceedings of the European Signal Processing Conference (EUSIPCO)*, 2009.

[21] A. Eryilmaz and R. Srikant, "Fair resource allocation in wireless networks using queue-length-based scheduling and congestion control," in *Proceedings of the IEEE Conference on Computer Communications (INFOCOM)*, 2005.

[22] H. Kim and Y. Han, "A proportional fair scheduling for multicarrier transmission systems," *IEEE Communications Letters*, vol. 9, no. 3, pp. 210–212, 2005.

[23] R. Jain, D. Chiu, and W. Hawe, "A quantitative measure of fairness and discrimination for resource allocation in shared computer systems," DEC, Research Report TR-301, 1984.

[24] T. Yoo and A. Goldsmith, "Optimality of zero-forcing beamforming with multiuser diversity," in *Proceedings of the IEEE International Conference on Communications (ICC)*, 2005.

[25] M. Schubert and H. Boche, *Interference Calculus – A General Framework for Interference Management and Network Utility Optimization*. Springer, 2012.

[26] M. Schubert, N. Vucic, and H. Boche, "SIR balancing for strongly connected interference networks – existence and uniqueness of a solution," in *Proceedings of the IEEE International Symposium on Wireless Communication Systems (ISWCS)*, 2010.

[27] N. Vucic and M. Schubert, "Fixed point iteration for max-min sir balancing with general interference functions," in *Proceedings of the IEEE International Conference on Acoustics Speech and Signal Processing (ICASSP)*, 2011.

[28] N. Vucic, S. Shi, and M. Schubert, "DC programming approach for resource allocation in wireless networks," in *Proceedings of the IEEE International Symposium on Modeling and Optimization in Mobile, Ad Hoc and Wireless Networks (WiOpt)*, 2010.

[29] K. Eriksson, S. Shi, N. Vucic, M. Schubert, and E. Larsson, "Globally optimal resource allocation for achieving maximum weighted sum rate," in *Proceedings of the IEEE Global Telecommunications Conference (GlobeCom)*, 2010.

[30] S. Hayashi and Z.-Q. Luo, "Spectrum management for interference-limited multiuser communication systems," *IEEE Transactions on Information Theory*, vol. 55, no. 3, pp. 1153–1175, 2009.

[31] *NS-3 Network Simulator*, Release 3.16 ed., 2012, [Online] *http://www.nsnam.org/*.

[32] S. M. Alamouti, "A simple transmit diversity technique for wireless communications," *IEEE Journal on Selected Areas in Communications*, vol. 16, no. 8, pp. 1451–1458, 1998.

[33] S. Catreux, L. J. Greenstein, and V. Erceg, "Some results and insights on the performance gains of MIMO systems," *IEEE Journal on Selected Areas in Communications*, vol. 21, no. 5, pp. 839–847, 2003.

[34] A. J. Paulraj, D. A. Gore, R. U. Nabar, and H. Bolcskei, "An overview of MIMO communications – a key to gigabit wireless," *Proceedings of the IEEE*, vol. 92, no. 2, pp. 198–218, 2004.

[35] G. J. Foschini, G. D. Golden, and R. A. Valenzuela, "Simplified processing for high spectral efficiency wireless communication employing multi-element arrays," *IEEE Journal on Selected Areas in Communications*, vol. 17, no. 11, pp. 1841–1852, 1999.

[36] *Spatial channel model for multiple input multiple output (MIMO) simulations (release 6)*, TR 25.996 v6.1.0 ed., 3GPP.

[37] "Spatial channel model for MIMO simulations – a ray based simulator based on 3GPP TR 25.996 v.6.1.0," 2008, [Online] *http://www.mathworks.com/matlabcentral/fileexchange/20911-spatial-channel-model-for-mimo-simulations-a-ray-based-simulator-based-on-3gpp-tr-25-996-v-6-1-0*.

[38] R. Pupala, Y. Yuan, Q. Bi, and L. Greenstein, "Downlink system throughput statistics for various mea configurations," *Journal of Communications*, vol. 6, no. 4, pp. 285–292, 2011.

[39] R. W. Heath Jr., S. Sandhu, and A. Paulraj, "Antenna selection for spatial multiplexing systems with linear receivers," *IEEE Communications Letters*, vol. 5, no. 4, pp. 142–144, 2001.

[40] G. Piro, N. Baldo, and M. Miozzo, "An LTE module for the ns-3 network simulator," in *Proceedings of the International ICST Conference on Simulation Tools and Techniques (SIMUTools)*, 2011.

[41] *Evolved Universal Terrestrial Radio Access (E-UTRA) – Physical layer procedures*, TS 36.213 v8.5.0 ed., 3GPP.

[42] S. Catreux, P. F. Driessen, and L. J. Greenstein, "Data throughputs using multiple-input multiple-output (MIMO) techniques in a noise-limited cellular environment," *IEEE Transactions on Wireless Communications*, vol. 1, no. 2, pp. 226–235, 2002.

[43] P. Mogensen, N. Wei, I. Z. Kovacs, F. Frederiksen, A. Pokhariyal, K. I. Pedersen, T. Kolding, K. Hugl, and M. Kuusela, "LTE capacity compared to the shannon bound," in *Proceedings of the IEEE Vehicular Technology Conference (VTC)*, 2007.

[44] *Further Advancements for Evolved Universal Terrestrial Radio Access (E-UTRA): Physical layer aspects*, TR 36.814 v1.2.1 ed., 3GPP.

[45] *Further Advancements for Evolved Universal Terrestrial Radio Access (E-UTRA): Physical layer aspects*, TR 36.814 v9.0.0 ed., 3GPP.

[46] J. Zhang, F. Römer, and M. Haardt, "Relay assisted physical resource sharing: Projection based separation of multiple operators (ProBaSeMO) for two-way relaying with MIMO amplify and forward relays," *IEEE Transactions on Signal Processing*, vol. 60, no. 9, pp. 4834–4848, 2012.

[47] M. Haardt, Z. K.-M. Ho, E. A. Jorswieck, E. Karipidis, J. Kibilda, J. Li, J. Lindblom, C. Scheunert, J. Sýkora, D. Gesbert, E. G. Larsson, and J. Zhang, "Adaptive and robust signal processing in multi-user and multi-cellular environments (initial)," SAPHYRE Project FP7-ICT-248001, Deliverable D3.1a, 2011.

[48] J. Zhang, M. Haardt, M. Filippou, R. Gangula, D. Gesbert, Z. K.-M. Ho, E. A. Jorswieck, E. Karipidis, E. G. Larsson, J. Li, J. Lindblom, C. Scheunert, J. Sýkora, L. Yu, and H. Zhang, "Adaptive and robust signal processing in multi-user and multi-cellular environments (final)," SAPHYRE Project FP7-ICT-248001, Deliverable D3.1b, 2012.

[49] J. Gora and S. Redana, "Resource management issues for multi-carrier relay-enhanced systems," *EURASIP Journal on Wireless Communications and Networking*, 2012.

[50] Y. Yang, H. Hu, J. Xu, and G. Mao, "Relay technologies for WiMax and LTE-advanced mobile systems," *IEEE Communications Magazine*, vol. 47, no. 10, pp. 100–105, 2009.

[51] J. Luo, A. Kortke, V. Jungnickel, F.-A. Böhner, A. Wolf, E. A. Jorswieck, J. Lindblom, E. Karipidis, E. G. Larsson, J. Li, J. Zhang, M. Haardt, P. Procházka, and J. Sýkora, "Test case implementation and evaluation on the demonstrator testbed (final)," SAPHYRE Project FP7-ICT-248001, Deliverable D6.3b, 2012.